THE JOURNAL OF BIOLOGICAL CHEMISTRY VOL. 287, NO. 44, pp. 36944–36967, October 26, 2012

Identification and Quantification of a New Family of Peptide Endocannabinoids (Pepcans) Showing Negative Allosteric Modulation at CB_1 Receptors*

Received for publication, May 16, 2012, and in revised form, August 23, 2012 Published, JBC Papers in Press, September 5, 2012, DOI 10.1074/jbc.M112.382481

Mark Bauer[‡§], Andrea Chicca[‡], Marco Tamborrini[§], David Eisen[¶], Raissa Lerner[‖], Beat Lutz[‖], Oliver Poetz[¶], Gerd Pluschke[§], and Jürg Gertsch[‡1]

From the [‡]Institute of Biochemistry and Molecular Medicine, National Center of Competence in Research TransCure, University of Bern, CH 3012 Bern, Switzerland, the [§]Swiss Tropical and Public Health Institute, Socinstrasse 57, CH 4002 Basel, Switzerland, the University of Basel, Petersplatz 1, CH 4003 Basel, Switzerland, the [¶]Natural and Medical Sciences Institute at the University of Tuebingen, 72770 Reutlingen, Germany, and the [‖]Institute of Physiological Chemistry, University Medical Center of the Johannes Gutenberg University Mainz, 55128 Mainz, Germany

Background: The α-hemoglobin-derived peptide RVDPVNFKLLSH was found to interact with cannabinoid CB_1 receptors.
Results: We generated mAbs against RVDPVNFKLLSH and identified a new family of endogenous peptides (Pepcans) that act as negative allosteric modulators at CB_1 receptors.
Conclusion: Allosteric ligands for CB_1 receptors are present in the brain.
Significance: Pepcans are a novel class of endogenous modulators of endocannabinoid signaling.

The α-hemoglobin-derived dodecapeptide RVD-hemopressin (RVDPVNFKLLSH) has been proposed to be an endogenous agonist for the cannabinoid receptor type 1 (CB_1). To study this peptide, we have raised mAbs against its C-terminal part. Using an immunoaffinity mass spectrometry approach, a whole family of N-terminally extended peptides in addition to RVD-Hpα were identified in rodent brain extracts and human and mouse plasma. We designated these peptides Pepcan-12 (RVDPVNFKLLSH) to Pepcan-23 (SALSDLHAHKLRVDPVNFKLLSH), referring to peptide length. The most abundant Pepcans found in the brain were tested for CB_1 receptor binding. In the classical radioligand displacement assay, Pepcan-12 was the most efficacious ligand but only partially displaced both [^{3}H]CP55,940 and [^{3}H]WIN55,212-2. The data were fitted with the allosteric ternary complex model, revealing a cooperativity factor value $\alpha < 1$, thus indicating a negative allosteric modulation. Dissociation kinetic studies of [^{3}H]CP55,940 in the absence and presence of Pepcan-12 confirmed these results by showing increased dissociation rate constants induced by Pepcan-12. A fluorescently labeled Pepcan-12 analog was synthesized to investigate the binding to CB_1 receptors. Competition binding studies revealed K_i values of several Pepcans in the nanomolar range. Accordingly, using competitive ELISA, we found low nanomolar concentrations of Pepcans in human plasma and ~100 pmol/g in mouse brain. Surprisingly, Pepcan-12 exhibited potent negative allosteric modulation of the orthosteric agonist-induced cAMP accumulation, [^{35}S]GTPγS binding, and CB_1 receptor internalization. Pepcans are the first endogenous allosteric modulators identified for CB_1 receptors. Given their abundance in the brain, Pepcans could play an important physiological role in modulating endocannabinoid signaling.

Cannabinoid CB_1 and CB_2 receptors are $G\alpha_{i/o}$ protein-coupled receptors with overall 48% amino acid sequence identity (1, 2). The CB_1 receptor is one of the most abundant receptors in brain (3) and the CB_2 receptor is primarily expressed in peripheral tissues (4). The known endogenous ligands for these receptors are the endocannabinoids derived from arachidonic acid, with arachidonoylethanolamide (anandamide; AEA)[2] and 2-arachidonoylglycerol (2-AG) being the best characterized endogenous agonists (5). Endocannabinoids are pleiotropic and exert multiple physiological effects via CB_1 and CB_2 receptors but also activate other receptors, such as GPR55 (G protein-coupled receptor 55), TRPV1 (transient receptor potential cation channel subfamily V member 1), and PPARs (6). The endocannabinoid system is involved in inflammation, pain, and metabolic disorders, and the modulation of CB receptors is a promising strategy for pharmacotherapy (6, 7). In 2007, Heimann *et al.* (8) reported that the α-hemoglobin-derived peptide hemopressin (Hpα) with the amino acid sequence PVNFKFLSH competitively binds to the [^{3}H]SR141716 binding site in isolated rat brain membranes. Based on *in vitro* func-

* This work was supported by Swiss National Science Foundation Grant 31003A_141174/1 (to J. G.), the National Center of Competence in Research TransCure, and the University of Bern Research Foundation.
[1] To whom correspondence should be addressed: Institute of Biochemistry and Molecular Medicine, University of Bern, Bühlstr. 28, CH-3012 Bern, Switzerland. Tel.: 41-316314-124; Fax: 41-316314-13737; E-mail: gertsch@ibmm.unibe.ch.

[2] The abbreviations used are: AEA, arachidonoylethanolamide; 2-AG, 2-arachidonoylglycerol; Aca, aminocaproic acid; ACN, acetonitrile; CP55,940, 2-((1*R*,2*R*,5*R*)-5-hydroxy-2-(3-hydroxypropyl) cyclohexyl)-5-(2-methyloctan-2-yl)phenol; Hp, hemopressin; HU-210, 3-(1,1-dimethylheptyl)-(−)-11-hydroxy-Δ^8-tetrahydrocannabinol; KLH, keyhole limpet hemocyanin; Pepcan, peptide endocannabinoid; PPAR, peroxisome proliferator-activated receptor; PTX, pertussis toxin; SR141716, 5-(4-chlorophenyl)-1-(2,4-dichloro-phenyl)-4-methyl-*N*-(piperidin-1-yl)-1*H*-pyrazole-3-carboxamide; TCM, ternary complex model; WIN55,212-2, (*R*)-(+)-[2,3-dihydro-5-methyl-3-(4-morpholinylmethyl)pyrrolo[1,2,3-de]-1,4-benzoxazin-6-yl]-1-napthalenylmethanone; GTPγS, guanosine 5′-*O*-(thiotriphosphate); GMBS, *N*-(γ-maleimidobutyryloxy)succinimide ester; C-ELISA, competitive ELISA; CB, cannabinoid; TRITC, tetramethylrhodamine isothiocyanate; BisTris, 2-[bis(2-hydroxyethyl)amino]-2-(hydroxymethyl)propane-1,3-diol; Fmoc, *N*-(9-fluorenyl)methoxycarbonyl.

tional experiments, they concluded that Hpα was CB_1 receptor-selective and showed CB_1 receptor inverse agonistic effects (8). *In vivo*, Hpα reduced food intake in rodents via CB_1 receptors (9). Later, the CB_1 receptor-active peptides RVD-Hpα and VD-Hpα were identified in mouse brain extracts using liquid chromatography tandem mass spectrometry (LC-MS/MS) (10). Based on functional assays, RVD-Hpα was suggested to interact rather selectively with CB_1 receptors, exerting partial agonistic effects, thus contrasting the effects with Hpα (10). Receptor binding assays were carried out with mouse cerebellar membranes. In 2010, the same group postulated that Hpα was probably a hot acid extraction artifact (11). Using LC-MS/MS, Gelman *et al.* (12) detected RVD-Hpα in mouse heart and brain tissues as well as in blood samples. Because CP55,940 shares an identical or at least closely overlapping CB_1 receptor binding site with the endocannabinoids AEA and 2-AG, as well as with the inverse agonist SR141716 (rimonabant) (13), it was suggested that Hpα partially interacts with the same binding pocket, also based on a recent *in silico* study using a CB_1 receptor homology model (14). However, experimental data showing binding interaction of Hpα and RVD-Hpα with CB receptor in defined expression systems are lacking.

The presence of putative CB_1 receptor binding peptides in the brain is intriguing and may suggest a functional role for such ligands. To date, all experiments have relied on LC-MS/MS data and extensive prior workup of post-mortem samples (10, 12). In this study, we have successfully raised monoclonal antibodies (mAbs) against the C-terminal part of RVD-Hpα to generate the necessary molecular tools to isolate and quantify CB_1 receptor-interacting peptides from mouse brain and mouse and human plasma samples. Apart from acidic extraction buffers, we used gentle extraction methods to reduce the probability of generating extraction artifacts. Using immunoaffinity mass spectrometry (MS) experiments, we were able to identify RVD-Hpα and N-terminally extended peptides of RVD-Hpα that we designated Pepcan-12 to -23, referring to the peptide length, but not Hpα and VD-Hpα. The peptides with the highest signal/noise ratios in immunoaffinity MS experiments were then synthesized and tested for CB_1 receptor binding in the classical radioligand displacement assay. Pepcan-12 showed the most potent saturable but only partial displacement of [^{3}H]CP55,950 and [^{3}H]WIN55,212-2, suggesting an allosteric modulation. The binding data were fitted with the ternary complex model (TCM), revealing a cooperativity factor value α of less than 1. In dissociation kinetic experiments, Pepcan-12 led to an increase of the dissociation rate constants. Both results support a negative allosteric modulation exerted by Pepcan-12 on the CB_1 receptor orthosteric binding site. In agreement, we show that Pepcans negatively modulate the efficacy of CB_1 receptor agonist-induced cAMP accumulation, [^{35}S]GTPγS binding, and CB_1 receptor internalization. At a functional level, Pepcan-12 strongly reduced the efficacy of 2-AG but not its potency. Pepcans were quantified in the nanomolar range from mouse brain and human plasma by competitive ELISAs. Overall, Pepcans represent the first endogenous allosteric modulators at CB_1 receptors, whereas several synthetic allosteric modulators have already been identified (15–18).

EXPERIMENTAL PROCEDURES

Peptide Synthesis

Peptides were synthesized using standard Fmoc solid-phase synthesis chemistry on a CS336 peptide synthesizer (CS Bio Co.) essentially as described before (19). Used resins were Rink Amide MBHA resin (peptides 2 and 4; Table 1) and Fmoc-His(Trt)-NovaSyn-TGT resin (peptides 1 and 3 and RVD-Hpα). Cysteine-containing Peptides were cleaved from the resin using TFA/triisopropylsilane/H_2O/1,2-ethanedithiol (94:1:2.5:2.5). Analytical and preparative HPLC analyses of the crude peptides were carried out on VWR HITACHI Elite LaChrom systems with symmetry C18 columns (3.5 μm, 4.6 × 100 mm for analytical HPLC and 5 μm, 19 × 100 mm for preparative HPLC) with flow rates of 1 and 25 ml/min, respectively. The peptides were identified by high resolution electrospray ionization mass spectrometry.

Peptide Coupling to Carrier Proteins and Generation of Fluorescently Labeled Peptides

A 5 mg/ml solution of peptide 1 (Table 1) in PBS, pH 7.2, was reduced with 5 mM tris(2-carboxyethyl)phosphine hydrochloride (Pierce) for 15 min at room temperature prior to incubation with either a 10 mg/ml solution of maleimide-activated mcKLH carrying a succinimidyl-4-(*N*-maleimidomethyl)cyclohexane-1-carboxylate cross-linker (Pierce) or a 10 mg/ml solution of ovalbumin (Pierce) preactivated with the heterobifunctional cross-linker *N*-(γ-maleimidobutyryloxy)succinimide ester (GMBS) for 2 h at room temperature. The ovalbumin-GMBS conjugate was synthesized using a 30-fold molar excess of sulfo-GMBS (Pierce) in activation buffer (0.1 M sodium phosphate, 0.15 M NaCl, pH 7.2) that was applied to a 5 mg/ml solution of ovalbumin and incubated for 60 min at room temperature. The conjugates were purified on an ÄKTA prime FPLC device with a 5-ml HiTrap desalting column (GE Healthcare), concentrated in Amicon-Ultra4 centrifugal filter units (Millipore), and analyzed with SDS-PAGE following Coomassie Brilliant Blue G-250 staining (Invitrogen). Introduction of fluorescein labels was done by a covalent postsynthetic coupling procedure of fluorescein 5-maleimide (Pierce) to the cysteine-containing peptides 1–4. Therefore, 2 mg of each peptide was dissolved in 200 μl of a 6.25 mg/ml solution of fluorescein 5-maleimide in *N*,*N*-dimethylformamide and incubated for 2 h in the dark at room temperature. After evaporation of *N*,*N*-dimethylformamide, the products were reconstituted in DMSO and purified and analyzed with preparative HPLC and electrospray ionization MS as described above.

Generation of Monoclonal Antibodies (mAbs)

Animals—For immunization experiments, three female 12-week-old (NZB×NZW)F1 hybrid mice (NZBNZW) from Harlan Laboratories were taken. Approval for animal experimentation was obtained from the responsible authorities, and all experiments were performed in strict accordance with the rules and regulations for the protection of animal rights laid down by the Swiss Bundesamt für Veterinärwesen.

Immunization, Generation of mAbs, and Antibody Purification—Mice were immunized subcutaneously with a keyhole limpet hemocyanin (KLH)-peptide conjugate (Table 1) formulated in Sigma Adjuvant System (Sigma). Starting on day 0, they received three doses of 50 μg of conjugate at 3-week intervals. Blood was collected before each immunization and 2 weeks after the final injection. The blood was centrifuged for 10 min (1500 $\times$ *g*) at 4 °C, and the serum was stored at −80 °C. Three days before the cell fusion, the mouse received an intravenous booster injection with 50 μg of the KLH-peptide conjugate in PBS. The generation of peptide-specific clones was done as described before (20). Cells secreting peptide-specific IgG were identified and screened by ELISA. Four hybridoma cell lines were selected and cloned twice by limiting dilution. mAbs were purified from sterile filtered culture supernatant by protein A affinity chromatography (HiTrap rProtein A FF, Amersham Biosciences) for IgG2a, IgG2b, and IgG3 isotypes and by protein G affinity chromatography (HiTrap Protein G, Amersham Biosciences) for IgG1 isotypes. Purified mAbs were dialyzed against PBS with Slide-A-Lyzer dialysis cassettes (Pierce), aliquoted, and stored at −80 °C.

Determination of Protein Concentration

Protein determinations of samples were carried out in duplicates on Polysorp microtiter plates (Nunc) using the bicinchoninicacid (BCA) protein assay reagent kit according to the manufacturer's protocol (Pierce). Calibration curves were prepared using defined concentrations of BSA. The protein complex absorption was detected at 562 nm.

ELISA

Determination of Antibody Titers—An ELISA was performed to test mouse sera for peptide-specific immune responses. Immulon 4 HBX microtiter plates (Dynex Technologies Inc.) were coated with 50 μl of a 10 μg/ml solution of an ovalbumin-peptide conjugate (Table 1) and ovalbumin (negative control) in PBS, pH 7.2, at 4 °C overnight. After washing once with PBS, 0.05% Tween, wells were blocked with 100 μl of 5% milk powder in PBS for 60 min at 37 °C. After another washing step, plates were incubated with 50 μl of eight 1:3 serial dilutions of mouse sera starting at 1:50 in PBS, 0.5% milk powder, 0.05% Tween 20 for 60 min at 37 °C. After three washing steps, plates were incubated with 50 μl of alkaline phosphatase-conjugated goat anti-mouse IgG (γ-chain-specific) antibodies (Sigma) for 60 min at 37 °C. Phosphatase substrate (1 mg/ml *p*-nitrophenyl phosphate (Sigma)) in 50 μl of buffer (0.14% Na_2CO_3, 0.3% $NaHCO_3$, 0.02% $MgCl_2$, pH 9.6) was added and incubated at room temperature after another three washing steps. The optical density (OD) of the reaction product was recorded after an appropriate time at 405 nm using a microplate reader (Sunrise, Tecan Trading AG).

NH_4SCN Competition ELISA—This ELISA was essentially performed as described before (21). After coating and blocking steps, mouse serum samples taken 3 weeks after the second and third immunization were added in triplicates at constant dilutions (at half-maximal titer). After a washing step, plates were incubated for 15 min with NH_4SCN diluted in 0.1 M Na_2HPO_4 buffer, pH 6, at the following molarities: 10, 7.5, 5, 2.5, 1.25, 0.63, and 0.31 M. Control wells were incubated with 0.1 M NaH_2PO_4 buffer without NH_4SCN. After washing, plates were developed as described above.

mAb Isotyping ELISA—Plates were coated with 50 μl of a 10 μg/ml solution of an ovalbumin-peptide conjugate (Table 1). After blocking and washing, 100 μl of selected hybridoma supernatants were added in duplicates and incubated for 60 min at 37 °C. After washing, plates were incubated for 60 min with alkaline phosphatase-conjugated goat anti-mouse antibodies specific for IgG (γ-chain-specific) (Sigma), IgG1, IgG2a, IgG2b, IgG3, λ, and κ (all from Southern Biotech), and plates were developed as described above.

Preparation of Color-coded Bead-based Peptide Arrays

To determine the minimal sequence required for antibody binding, a bead-based peptide array was prepared as previously described (22–24). The array consisted of the RVD-Hpα peptide (RVDPVNFKLLSH), a carboxamide version of the RVD-Hpα peptide, and 22 truncated peptides. Truncated peptides started from the C or the N terminus of the antigen. C-terminally truncated peptides were synthesized in the form of carboxamides, whereas N-terminal truncations had a carboxyl group at the C terminus. For immobilization purposes, two hydrophilic spacers (8-amino-2,6-dioxaoctanoic acid) and a cysteine were added to the N terminus of all peptides. All peptides were purchased from Intavis. Each of the 24 peptides was conjugated onto a distinct color-coded bead population. For the epitope mapping, 500 beads of each population were mixed to give a peptide array. BSA-coated beads served as a negative control.

Epitope Mapping of mAbs

30 μl of the premixed bead-based peptide array (500 beads/population) were used to assess the minimal epitopes of the RVD-Hpα peptide-specific mAbs. The mixture of beads was transferred to 96-well filter plates (Merck Millipore) and incubated with 30 μl of the respective RVD-Hpα peptide-specific antibody (1 μg/ml) for 60 min at 23 °C and 650 rpm. Subsequently, beads were washed two times with 100 μl of PBS, 0.05% Tween by vacuum filtration (Merck Millipore). Finally, the formation of the antibody-peptide complexes was detected by incubation with 30 μl of anti-mouse IgG-phycoerythrin conjugate (2.5 μg/ml; Jackson ImmunoResearch Inc.) for another 45 min at 23 °C and 650 rpm. Following two further washing steps, the beads were resuspended in 100 μl of blocking reagent for ELISA (Roche Applied Science), 0.1% Tween. Read-out of the bead type-specific reporter fluorescence was performed on a Luminex IS 100 system (Luminex Corp.).

Peptide Extraction from Brain and Plasma Samples

From Rodent Brain Tissues—For brain peptide extractions female 12-week-old NMRI mice were used (Charles River). Hamster and rat brains were a kind gift from the group of Prof. Jennifer Keiser at the SwissTPH. From the sacrificed mice, brains were removed aseptically, immediately frozen in liquid nitrogen, and stored at −80 °C. Brains were homogenized (2 $\times$ 6000 rpm, 5-min break with cooling on ice) with a Precellys24 tissue homogenizer (Bertin Technologies) in 2-ml tubes containing 1.4-mm ceramic beads (Bertin Technologies) either

immediately in extraction buffer for Western blot and immunoaffinity MS experiments or first in double-distilled H_2O for spike and recovery experiments following an acetonitrile/H_2O (2:1) (ACN 66%) extraction for peptide quantification in competitive ELISA experiments. All brain extraction approaches contained 1× complete protease inhibitor mixture (Roche Applied Science). The different extraction buffers used were PBS, pH 7.2, ACN/H_2O 1:1 (ACN 50%), ACN 66%, 10 mM HCl, and 100 mM acetic acid (AcOH). Rodent brains were homogenized at 0.5 g wet weight/ml extraction buffer with subsequent centrifugation for 5 min at 12,000 × *g*. The supernatants of the acid extractions were neutralized with NaOH, and the supernatants of the ACN extractions were evaporated to dryness in a SpeedVac (CentriVap Concentrator and CentriVap Cold Trap, Labconco) at 60 °C. All extracts were stored at −80 °C.

From Human and Mouse Plasma—Human blood samples were drawn with the Vacuette blood collection system (Greiner Bio-One) from healthy female and male volunteers (age 25–30 years) with EDTA as anticoagulant. Mouse blood samples were collected by cardiac puncture with heparin as anticoagulant. The blood samples were immediately centrifuged at 1500 × *g* for 10 min at 4 °C, and the supernatant was stored at −80 °C. Plasma peptide extraction was based on a previous method (7). For peptide extraction, ACN was added to thawed plasma (diluted 1:1 with PBS, 0.5% BSA, 0.05% Tween, pH 7.2) in a 2:1 ratio (ACN 66%) or 1:1 ratio (ACN 50%) and incubated for 60 min at room temperature. After centrifugation at 12,000 × *g* for 5 min, the supernatant was evaporated to dryness in the SpeedVac at 60 °C. The dried samples were stored at −80 °C.

SDS-PAGE and Western Blot Experiments

For SDS-PAGE, 100 μl of each mouse brain extract (the ACN brain extracts were reconstituted in 1 ml of PBS, pH 7.2) was diluted 1:1 in 50 μl of LDS 4× sample buffer, 20 μl of 10× reducing agent (Invitrogen), and 30 μl of double-distilled H_2O and heated at 70 °C for 10 min. Proteins were separated on a 4–12% BisTris Zoom gel (Invitrogen) and transferred to a nitrocellulose filter by dry blotting on the iBlot system (Invitrogen). Blots were blocked with 5% milk powder in PBS at 4 °C overnight. The blots were cut into stripes and incubated with mAbs in PBS, 0.5% milk powder, 0.05% Tween for 2 h at room temperature. After four washing steps with PBS, 0.1% Tween, stripes were incubated with goat anti-mouse IgG horseradish peroxidase-conjugated antibodies (Bio-Rad) for 60 min. After washing, blots were developed using the ECL system according to the manufacturer's instructions (Pierce).

Competitive Western Blot Experiments

For competitive experiments, cut stripes were incubated with six serial 1:5 dilutions of the synthetic peptide RVD-Hpα (Table 1) starting at 10 μM. As negative control, the similar sized bovine peptide [Val^5]angiotensin I (Sigma) was used at a concentration of 10 μM. The mAbs were used at a concentration of 10 μg/ml, and the blots were developed as described above ($n = 3$).

Immunoaffinity MS and MS/MS Experiments

Brain and plasma extracts were reconstituted in the initial sample volume using PBS, 0.3% *N*-octyl glucoside, vortexed for 1 min, and sonicated until they were completely resolved. 100 μl were incubated with 1 μg of anti-RVD-Hpα antibody for 60 min at room temperature in a PCR microtiter plate (ThermoFisher). Paramagnetic protein G-coated beads (Dynabeads) were washed four times with PBS, 0.3% *N*-octyl glucoside, and 5 μl of the bead suspension were added to each sample. After a 60-min incubation at room temperature, the beads were washed four times and eluted in 1% formic acid as described previously (24, 25). 1 μl of each sample was spotted in triplicates onto a Prespotted HCCA AnchorChip (Bruker Daltonics). The MALDI MS readout was performed on an Ultraflex III MALDI-TOF/TOF (Bruker Daltonics) running in positive ion reflectron mode. Peptides were identified by *de novo* sequencing using tandem mass spectrometry (MS/MS). External calibration was automatically performed with the prespotted MALDI calibrants using the flexAnalysis version 3.0.92.0 software.

Cell Culture

All cell lines were cultured in medium supplemented with 10% FBS, penicillin, streptomycin, amphotericin B (all from Sigma) at 37 °C and 5% CO_2. CHO-K1 (CHO) and CHO-K1 cells stably transfected with human CB_1 (CHO-*h*CB_1) or human CB_2 receptors (CHO-*h*CB_2), were obtained from Dr. Michael Detheux (Euroscreen S.A., Brussels, Belgium) and cultured in RPMI 1640 (Invitrogen) with 400 μg/ml G418 (Sigma). HL60 cells (human promyelocytic leukemia cells; ATCC CCL-240) were cultured in IMDM (ATCC). N18TG2 cells (ACC-103, DSMZ, Germany) were cultured in DMEM with 100 μM 6-thioguanine (Sigma). HEK293 cells stably transfected with human TRPV1 (a kind gift from Ken Mackie, Indiana University, Bloomington, IN) or human GPR55 receptors (a kind gift from Gábor Pethö, University of Pécs, Hungary) were cultured in RPMI 1640.

Receptor Binding Studies

Equilibrium Radioligand Binding Assays—Radioligand binding assays using [^{3}H]CP55,940 and [^{3}H]WIN55,212-2 were performed with CB_1 receptor membrane preparations as reported previously (26, 27). Briefly, 18 μg of crude membranes of CHO-*h*CB1 cells (prepared as described previously (28)) were resuspended in 500 μl of binding buffer (50 mM Tris-HCl, 2.5 mM EDTA, 5 mM $MgCl_2$, 0.5 mg/ml fatty acid-free BSA, pH 7.4) in silanized glass tubes and co-incubated with different concentrations of Pepcans and 0.5 nM [^{3}H]CP55,940 (168 Ci/mmol) or 2.5 nM [^{3}H]WIN55,212-2 (40 Ci/mmol) for 60 min at 30 °C under shaking. Pepcans were directly diluted from the DMSO stock solutions in assay buffer (1:100) to the final concentrations. Because micromolar concentrations of Pepcans in buffer (fractional dilution of DMSO stock) may cause aggregation and loss of free peptides, the means of administration of Pepcans to cells was important. Nonspecific binding of the radioligand was determined in the presence of 10 μM WIN55,512-2 or CP55,940, respectively. Nonspecific binding was around 5%. After the incubation time, membrane suspensions were rapidly filtered through a 0.1% polyethyleneimine presoaked 96-well

microplate bonded with GF/B glass fiber filters (UniFilter-96 GF/B, PerkinElmer Life Sciences) under vacuum and washed 12 times with 167 μl of ice-cold washing buffer (50 mM Tris-HCl, 2.5 mM EDTA, 5 mM $MgCl_2$, 0.5% fatty acid-free BSA, pH 7.4). Filters were added with 40 μl of MicroScint20 scintillation liquid, and radioactivity was measured with the 1450 MicroBeta Trilux top counter (PerkinElmer Life Sciences). Data were collected from 3–5 independent experiments, each performed in triplicate, and the nonspecific binding was subtracted. The results are expressed as a percentage of vehicle-treated samples.

Dissociation Kinetic Studies Using Isotopic Dilution—Dissociation kinetics experiments were performed as described before (16, 29). Briefly, 18 μg of membranes of CHO-*h*CB1 cells were resuspended in 500 μl of binding buffer (50 mM Tris-HCl, 2.5 mM EDTA, 5 mM $MgCl_2$, 0.5 mg/ml fatty acid-free BSA, pH 7.4) in silanized glass tubes and incubated with 0.5 nM [^{3}H]CP55,940 for 60 min at 30 °C under shaking. Radioligand dissociation was initiated by the addition of 1 μM WIN55,212-2 in the presence of 300 nM Pepcan-12 or solvent (DMSO) and incubated for 1–120 min, at 30 °C. Nonspecific binding of the radioligand was determined in the presence of 10 μM CP55,940. After the incubation time, membrane suspensions were rapidly filtered through a 0.1% polyethyleneimine presoaked 96-well microplate bonded with GF/B glass fiber filters and washed as described above.

Equilibrium Binding Studies Using a Fluorescently Labeled Pepcan-12 Derivative—The equilibrium dissociation constant (K_d value) of the fluorescein-labeled Pepcan-12 derivative Pepcan-F4 (Table 1) was determined using CHO-*h*CB_1 cells. Equilibrium saturation binding was determined experimentally, and maximal specific binding (saturation) was reached already at 5 min at 37 °C. Different concentrations of Pepcans and 100 nM Pepcan-F4 were incubated together with 10^5 cells suspended in 200 μl of binding buffer (50 mM Tris-HCl, 2.5 mM EDTA, 5 mM $MgCl_2$, and 0.5% fatty acid-free BSA, pH 7.4) in silanized plastic tubes, under shaking for 60 min at 37 °C. After centrifugation at 4 °C and washing with ice-cold binding buffer, the cells were resuspended in ice-cold PBS and transferred into 96-well black plates, where the fluorescence intensities were measured using a Tecan Farcyte reader (485-nm excitation/535-nm emission). The specific binding was determined after washing and subtracting the nonspecific fluorescence calculated in parallel experiments carried out in non-transfected CHO cells.

Competitive Enzyme-linked Immunosorbent Assay (C-ELISA)

Characterization of mAb 1A12—Binding affinity of the mAb 1A12 toward the C-terminal truncated peptides RVDPVNFKLL and RVDPVNF; the N-terminal extended peptides KLRVDPVNFKLLSH, HKLRVDPVNFKLLSH, HAHKLRVDPVNFKLLSH, and SDLHAHKLRVDPVNFKLLSH (all from Genscript); rat hemopressin (PVNFKFLSH) (Tocris Bioscience); the hemoglobin β-chain derived peptide HVDPENFRLLGN (Genscript); and SDS-PAGE purified, 2× crystallized bovine hemoglobin (Sigma) was determined and compared with the binding affinity toward RVD-Hpα (RVDPVNFKLLSH) with or without ACN extraction. As negative control, the peptide [Val^5]angiotensin I (Sigma) was used. Maxisorp microtiter plates (Nunc) were coated with 50 μl of a 10 ng/ml solution of an ovalbumin-peptide conjugate (Table 1) as described above. After blocking and washing, 11 1:3 serial dilutions starting at a 10 μM concentration of the analytes in PBS, 0.5% BSA, 0.05% Tween (assay buffer) and each containing 20 ng/ml of mAb 1A12 were incubated for 2 h at room temperature. After washing, plates were incubated with 50 μl of goat anti-mouse IgG horseradish peroxidase-conjugated antibodies (Bio-Rad) for 60 min at room temperature. Plates were developed with 50 μl of 3,3′,5,5′-tetramethylbenzidine substrate (Pierce) after washing. The reaction was stopped after 15 min with 50 μl of 2 M H_2SO_4, and the OD of the reaction product was recorded at 450 nm. For ACN extraction, samples were processed as described above. Briefly, samples were incubated with ACN/H_2O in a ratio of 1:1 (ACN 50%) or 2:1 (ACN 66%), incubated, and centrifuged, and the supernatant was evaporated to dryness in the SpeedVac. Pellets were reconstituted in assay buffer.

Peptide Quantification from Mouse Brain Tissue and Human Plasma Samples—For peptide quantification, a C-ELISA as described above was used with ACN 66% extraction. Twelve calibrators containing 1000, 200, 100, 50, 25, 12.5, 6.25, 3.13, 1.56, 0.78, 0.39, and 0.16 nM RVD-Hpα were prepared in assay buffer and extracted with ACN/H_2O in a ratio 2:1 and processed as shown above. NMRI mouse brain extracts and human plasma samples for spike and recovery experiments were diluted 1:1 in assay buffer prior to ACN 66% extraction. Samples for quantification were treated the same way. The dried samples were reconstituted in the initial volume in assay buffer.

Measurement of cAMP Accumulation

For cAMP measurement, we used the GloSensor™ luminescence assay (Promega) for detecting cAMP levels in live cells. Therefore, CHO-*h*CB_1 and wild-type CHO cells were stably transfected with the pGloSensor™-22F plasmid using Lipofectamine 2000 in OptiMEM I reduced serum medium (both from Invitrogen). Screening of positive clones and assay development were according to the manufacturer's instructions. For measurement of cAMP accumulation, 3×10^4 cells were grown in RPMI 1640 medium overnight in white 96-well microtiter plates (Greiner, clear bottom) After incubation with 2% GloSensor cAMP reagent (Promega) in 200 μl of medium for 2 h at 37 °C, 1 μl of compounds diluted in DMSO were added, and luminescence was measured after 3 min of incubation on a 1450 MicroBeta TriLux counter. Competitors and agonists were applied in succession (3-min preincubation for SR141716). Results are expressed as percentages of vehicle control after division of preread responses, measured directly before adding compounds, to account for well-to-well variance.

Agonist-stimulated [^{35}S]GTPγS Binding

C57BL/6N male mice (3–6 months old) were anesthetized with isoflurane and decapitated. Brains were quickly removed, and cerebelli were dissected on ice and homogenized in ice-cold homogenization buffer (50 mM Tris-HCl, pH 7.4, 0.2 mM EGTA, 3 mM $MgCl_2$, 50 μM phenylmethanesulfonyl fluoride (PMSF), 1× Complete protease inhibitor (Roche Applied Science)) using a glass homogenizer. Protein concentration was determined by using a BCA assay (Thermo Scientific). Homo-

genates were aliquoted and stored at −80 °C until use. Agonist-stimulated [^{35}S]GTPγS binding assays were carried out as described previously (30). Briefly, cerebellar brain homogenates (5–6 μg) were diluted in assay buffer (50 mM Tris-HCl, pH 7.4, 3 mM $MgCl_2$, 0.2 mM EGTA, 100 mM NaCl) and incubated with 0.05 nM [^{35}S]GTPγS (1250 Ci/mmol; PerkinElmer Life Sciences) containing 30 μM GDP and 0.5% fatty acid-free BSA in a final volume of 1 ml. Compounds, prepared as DMSO stocks, were sequentially diluted in assay buffer and incubated for 60 min at 30 °C. Nonspecific binding was determined in the presence of 10 μM GTPγS, and specific binding was defined as total binding minus nonspecific binding. Bound [^{35}S]GTPγS was harvested by vacuum filtration over Whatman GF/B filters with a Brandel Cell Harvester and transferred to scintillation vials containing Aquasafe 300 plus (Zinsser Analytic) scintillation mixture. Radioactivity was measured by liquid scintillation counting using Tri-Carb 2800 TR (PerkinElmer Life Sciences). Data are expressed as percentage of basal specific binding.

Receptor Internalization Studies

The assessment of the surface expression of CB_1 receptors was performed using CHO-K1 cells stably transfected with human CB_1 receptors as described before (31). Compounds diluted in DMSO were added to 10^5 cells and incubated for 60 min at 37 °C at a final concentration of 1 μM.

Assessment of Peptide Aggregation

Peptide aggregation was measured by exploiting the competitive ELISA for peptide quantification described above, however without ACN extraction. For each peptide, a low (10 nM) and a high concentration (1 μM) were incubated in RPMI 1640 medium supplemented with 10% FCS, penicillin, streptomycin, and amphotericin B for 60 min at 37 °C and subsequently centrifuged in ultrafiltration tubes with 2,000 (Vivaspin 2 Hydrosart) and 3,000 (Vivaspin 2 Polyethersulfone) molecular weight cut-off, respectively, at 4000 × *g*. The filtrates of the 1 μM peptide solutions were diluted 1:100 in filtered medium, and both the 10 nM and the 1:100 diluted 1 μM peptide dilutions were quantified in the C-ELISA.

AEA and 2-AG Hydrolysis Assays

[*ethanolamine*-1-^{3}H]Anandamide (40–60 Ci/mmol) and [1,2,3-^{3}H]2-arachidonyl glycerol (20–40 Ci/mmol) were obtained from American Radiolabeled Chemicals Inc. (Saint Louis, MO). Different concentrations of Pepcan-12 or 1 μM PMSF (as the positive control) in a 2.5-μl volume (DMSO) were preincubated at 37 °C for 20 min with 195 μl of diluted pig brain homogenate in 10 mM Tris-HCl and 1 mM EDTA, pH 7.6 (corresponding to 200 μg of total protein) and 1% (w/v) fatty acid-free BSA (Sigma). Successively, 2.5 μl of non-radioactive anandamide and [*ethanolamine*-1-^{3}H]anandamide (40–60 Ci/mmol) mixture were added to the homogenate (final concentration in the assay was 2 μM) and incubated for 10 min at 37 °C under shaking. After the incubation time, 400 μl of a methanol/chloroform mixture (1:1, v/v) was added at each sample, vigorously vortexed, and centrifuged at 10,000 rpm for 10 min at 4 °C to separate aqueous and organic phases. The radioactivity associated with the hydrolytic formed [^{3}H]ethanolamine was measured upon the addition of 3 ml of Ultima Gold scintillation liquid (PerkinElmer Life Sciences) to the aqueous phase, using a Tri-Carb 2100 TR scintillation counter (PerkinElmer Life Sciences). Data were collected, and FAAH activity was expressed as a percentage of vehicle-treated samples. For 2-AG hydrolysis, 195 μl (corresponding to 200 μg of total protein) of diluted pig brain homogenate in 10 mM Tris-HCl, 1 mM EDTA plus 0.1% (w/v) fatty acid-free BSA, pH 7.4, was preincubated for 30 min at 37 °C with different concentrations of Pepcan-12 and 1 μM JZL184 as the positive control for the maximal 2-AG hydrolysis inhibition via MAGL. After the preincubation, 2.5 μl of nonradioactive 2-AG and [1,2,3-^{3}H]2-AG (60 Ci/mmol) mixture were added to the homogenate (final concentration in the assay was 10 μM) and incubated for 10 min at 37 °C under shaking. Successively, 400 μl of a methanol/chloroform mixture (1:1, v/v) were added and, after vigorous vortexing, aqueous and organic phases were separated by centrifugation at 10,000 rpm for 10 min at 4 °C. The radioactivity associated with the [^{3}H]glycerol formation was measured upon the addition of 3 ml of Ultima Gold scintillation liquid (PerkinElmer Life Sciences) to the aqueous phase, using a Tri-Carb 2100 TR scintillation counter (PerkinElmer Life Sciences). Data were collected from different experiments, and results were expressed as [^{3}H]glycerol formation in a percentage of vehicle-treated samples.

Data Analysis

All data analyses were done by using GraphPad Prism 5 software.

Radioligand Binding Assays—Competition binding curves of orthosteric ligands were analyzed using a three-parameter one-site competitive binding equation.

$$Y = Bottom + \frac{(Top - Bottom)}{(1 + 10^{([A] - \log IC_{50})})} \quad \text{(Eq. 1)}$$

A relationship between the IC_{50} and the K_i value is given by the Cheng-Prusoff equation (32),

$$K_i = \frac{IC_{50}}{1 + \frac{[R]}{K_d}} \quad \text{(Eq. 2)}$$

where Y represents fractional specific binding, $[A]$ is the logarithm of the concentration of cold orthosteric competitor, *Top* and *Bottom* represent plateau values in units of the *y* axis, $[R]$ is the concentration of the hot ligand used (0.5 nM for [^{3}H]CP55,940 and 2.5 nM for [^{3}H]WIN55,212-2), and K_d values are equilibrium dissociation constants of the hot ligand determined in former saturation binding experiments (0.5 nM for [^{3}H]CP55,940 and 2.5 nM for [^{3}H]WIN55,212-2). The K_i values were determined by nonlinear regression.

The interaction between radioligands and Pepcan-12 (modulator titration curves) was analyzed using the following allosteric TCM equation as introduced before (16),

$$Y = \frac{[A]}{[A] + \frac{K_A(1 + [B]/K_B)}{1 + \alpha[B]/K_B}} \quad \text{(Eq. 3)}$$

where $[A]$ and $[B]$ represent concentration of orthosteric and allosteric ligands, respectively; α is the cooperativity factor; K_A and K_B are the respective equilibrium dissociation constants; $[A]$ and K_A were fixed as constants (see above for values); and α and K_B were determined by nonlinear regression.

Dissociation Kinetics—The dissociation kinetic experiment was analyzed using the following two-phase exponential decay model introduced before (16),

$$Y = Plateau + Span1 \times e^{-k_1 t} + Span2 \times e^{-k_2 t} \quad \text{(Eq. 4)}$$

where *Span1* and *Span2* represent the percentage of each phase; k_1 and k_2 are the dissociation rate constants for the components defined by *Span1* and *Span2*, respectively; and *Plateau* is the minimal asymptotic value. Values were determined by nonlinear regression with constraint of the minimal plateau value to 0 to account for the subtraction of nonspecific binding.

Equilibrium Binding Studies Using a Fluorescently Labeled Pepcan-12 Derivative—The K_d value of Pepcan-F4 for $h\mathrm{CB}_1$ was determined by a nonlinear fit using the following one-site specific binding model,

$$Y = \frac{B_{max} \times [X]}{K_d \times [X]} \quad \text{(Eq. 5)}$$

where B_{max} represents maximum specific binding, and $[X]$ is the concentration of Pepcan-F4. IC_{50} values were determined by a four-parameter dose-response curve with variable slope (here the IC_{50} values used were the concentrations of competitors displacing 50% of Pepcan-F4 (33). Derived from the K_d value of Pepcan-F4 for $h\mathrm{CB}_1$ (37 nM) and the IC_{50} value, the K_i value of each competitor was calculated by using the Cheng-Prusoff equation (see above).

Functional Data Analysis—EC_{50} (half-maximal effective concentration) values from competitive ELISA, cAMP assay, and [^{35}S]GTPγS binding assay data were obtained by using a four-parameter dose-response (stimulation or inhibition) model with variable slope,

$$Y = basal + \frac{(E_{max} - basal)}{(1 + 10^{((\log EC_{50} - [X]) \times n_H)})} \quad \text{(Eq. 6)}$$

where $[X]$ represents the logarithm of the concentration of drug used; n_H is Hill slope, and E_{max} is maximal efficacy/maximal response. Depending on the assay, pEC_{50} or pIC_{50} (negative $\log EC_{50}$ or negative $\log IC_{50}$) values are shown.

The Schild analysis was chosen to analyze competitive antagonism in the cAMP accumulation assay and was done as described in literature (15, 34, 35). There is a relationship between the dextral shift of agonist curves incubated with increasing concentrations of competitor (expressed as concentration ratio (*CR*) values defined by dividing EC_{50} values of agonist curves with increasing competitor concentrations by the EC_{50} value of the agonist curve without competitor) and the concentration of competitor, $[A]$, and its equilibrium dissociation constant K_A by the Schild equation,

$$\log(CR - 1) = \log[A] - \log K_A \quad \text{(Eq. 7)}$$

TABLE 1
Synthesized peptides, peptide-protein and peptide-fluorophore conjugates

Name	Sequence	m/z [MH^+][a]
1	C-Aca[b]-Aca-RVDPVNFKLLSH	1753.97
2	RVDPVNFKLLSH-Aca-Aca-C	1752.99
3	C-RVDPVNFKLLSH	1527.81
4	RVDPVNFKLLSH-C	1526.83
RVD-Hpα (Pepcan-12)	RVDPVNFKLLSH	1424.79
	KLH[c]-C-Aca-Aca-RVDPVNFKLLSH	
	Ova[d]-C-Aca-Aca-RVDPVNFKLLSH	
Pepcan-F1	FL[e]-C-RVDPVNFKLLSH	1954.87
Pepcan-F2	RVDPVNFKLLSH-C-FL	1953.89
Pepcan-F3	FL-C-Aca-Aca-RVDPVNFKLLSH	2181.04
Pepcan-F4	RVDPVNFKLLSH-Aca-Aca-C-FL	2180.06

[a] Measured mass from ESI-MS (charge +1).
[b] Aca, aminocaproic acid.
[c] Keyhole limpet hemocyanine.
[d] Ovalbumin.
[e] FL, fluorescein.

Linear regression delivers estimates about the slope (unity slope for competitive antagonists) and the K_A value of the competitor (35).

Statistics

Results are expressed as mean values ± S.D. or mean values ± S.E. for each examined group. Statistical significance of differences between groups was determined by the unpaired Student's *t* test or one-way analysis of variance followed by Dunnett's post hoc test with the GraphPad Prism 5 software. Outliers in a series of identical experiments were determined by Grubb's test (extreme studentized deviate (ESD) method) with α set to 0.05. As described before (16), an extra-sum-of-squares test (F test) was used to determine if the exponential two-phase decay model is superior to a corresponding one-phase decay model.

For the quantification of Pepcans from brain tissue and plasma, descriptive statistics (mean, S.D. values, percentage coefficients of variation, differences from theoretical, and percentage recovery values) were calculated for the calibrators and the samples used for spike and recovery experiments.

RESULTS

Generation and Characterization of mAbs Specific for CB Receptor Binding Peptides—Our initial strategy was to raise mAbs recognizing the reported endogenous brain peptides RVD-Hpα (RVDPVNFKLLSH), VD-Hpα, and Hpα (hemopressin), which differ only in their N termini. We therefore generated mAbs against the C-terminal part with the intention of detecting all three peptides. Mice were immunized with a peptide conjugate in which RVD-Hpα was N-terminally coupled to KLH (Table 1). We have chosen the mouse/human RVD-Hpα sequence that differs from the sequence in rats (RVDPVNFKFLSH) by a single amino acid substitution at position 9 (Phe → Leu). The peptide was conjugated to KLH via two aliphatic aminocaproic acid (Aca) straight-chain spacers and a terminal cysteine residue for thiol coupling chemistry (Table 1). Autoimmune-prone NZBNZW mice, which have been reported to be capable of generating high affinity antibodies against self-antigens (36) were chosen for immunization. To select for the mouse generating the highest affinity antibodies, we determined the avidity index with an NH_4SCN competition ELISA (Fig. 1*A*). All mice showed affinity maturation in the

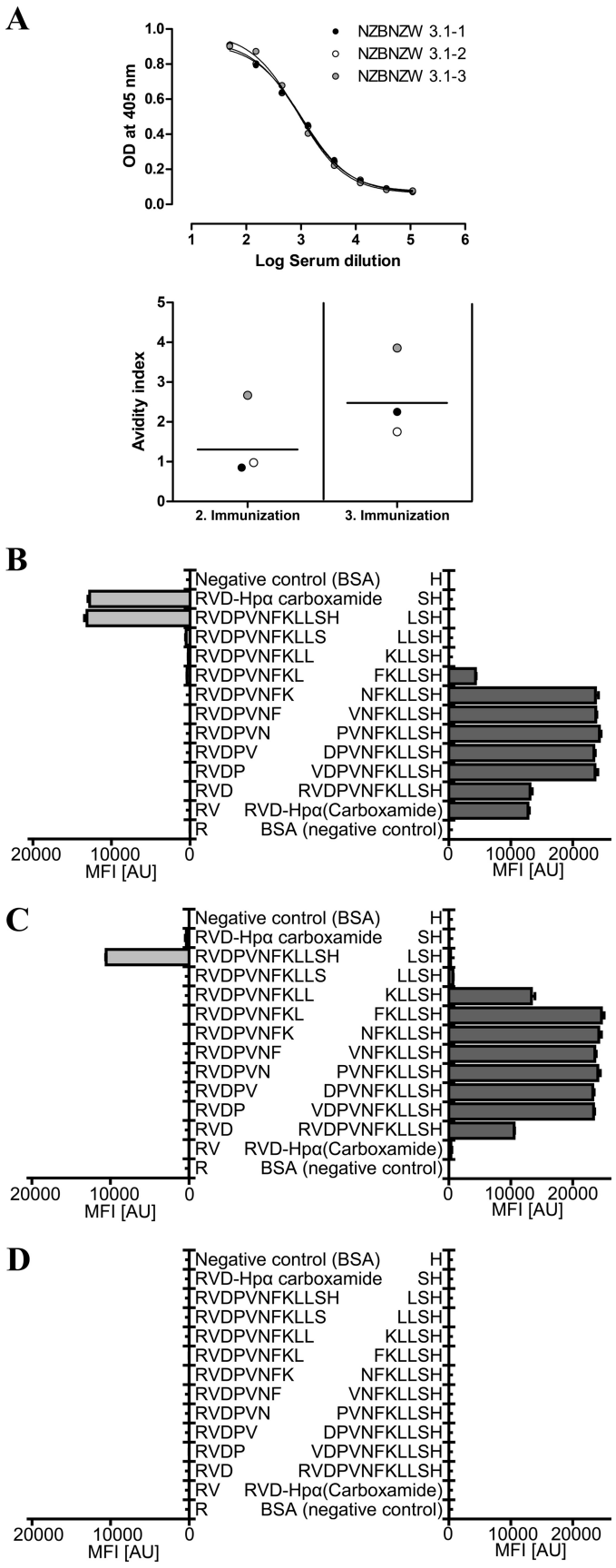

FIGURE 1. *A*, peptide-specific immune responses to antigen KLH-C-Aca-Aca-RVDPVNFKLLSH (Table 1) of three NZBNZW mice (after the third immunization) determined by ELISA ($n = 1$). *Bottom*, results from NH_4SCN elution ELISA of the corresponding mouse sera taken 3 weeks after the second and third immunization. The avidity index corresponds to the molar NH_4SCN concentration that displaces 50% of binding toward coated ovalbumin-C-Aca-Aca-RVDPVNFKLLSH (Table 1) of sera used at half-maximal titer concentrations of individual animals. The *line* displays the geometric mean of IC_{50} values that were determined in triplicate experiments. *B–D*, minimal epitopes of RVD-Hpα-specific mAbs. Color-coded bead-based peptide arrays were employed to determine the minimal epitopes of the RVD-Hpα specific mAbs. The array was fabricated from a set of N-terminally and C-terminally truncated versions of the RVD-Hpα peptide. Mean fluorescence intensities (*MFI*) ($n = 3$) are plotted against the respective peptide sequences in a *bar chart*. Results for C-terminally truncated peptides are displayed in *light gray* (*left*) and for N-terminally truncated peptides in *dark gray* (*right*). BSA-coated beads served as control. Representative results for mAb 1A12 (*B*) and mAb 7A5 (*C*) are shown. Results for reagent control are shown in *D*. Results indicate an epitope of mAb 1A12 containing the peptide sequence FKLLSH (*B*). *C*, epitope mapping of mAb 7A5 revealed a neoepitope bearing the sequence KLLSH. Minimal epitopes of four mAbs are indicated in Table 2. *Error bars*, S.D., *AU*, arbitrary units.

TABLE 2
Results of four mAbs in epitope mapping and C-ELISA experiments

mAb	Isotype	Epitope	Neoepitope[a]	pIC_{50}± S.E.[b]
1A12	IgG2a, κ	FKLLSH		8.02 ± 0.02
2C11	IgG2b, κ	FKLLSH		7.33 ± 0.12
7A5	IgG2a, κ		KLLSH	6.33 ± 0.07
8D4	IgG1, κ		FKLLSH	6.84 ± 0.02

[a] Neoepitopes contain the charge of the C terminus as an essential part of their epitope. mAbs 7A5 and 8D4 recognized RVD-Hpα with a free C terminus but not the carboxamide derivative (Fig. 1).

[b] pIC_{50} values were estimated by nonlinear regression analysis of the synthetic peptide RVDPVNFKLLSH competing for the binding of the mAb toward the corresponding ovalbumin-peptide conjugate (Table 1) in C-ELISA under optimized conditions (2C11 (2 ng/ml), 7A5 (10 ng/ml), 8D4 (50 ng/ml); for experiments with 2C11 and 7A5, 50 μl of 15 ng/ml ovalbumin-peptide conjugate were coated, and for 8D4, 50 μl of 150 ng/ml were used).

course of the three immunizations. We selected the mouse showing the highest avidity index against peptide RVD-Hpα for the generation of mAbs. The minimal epitopes of four generated hybridoma clones were determined in a bead-based peptide array assay and are representatively shown for mAbs 1A12 and 7A5 in Fig. 1, *B* and *C*, respectively. Details for the binding properties of four mAbs are provided in Table 2.

Because RVD-Hpα was reported to occur abundantly in rodent brain (10, 12), we performed Western blot experiments of mouse brain extracts using different extraction buffers. These included acidic extractions (10 mM HCl and 100 mM AcOH) as well as chemically more gentle extractions using PBS, pH 7.2, ACN/H_2O 1:1 (ACN 50%) and 2:1 (ACN 66%). The use of gentle extraction buffers was motivated by the fact that acid extraction was reported to create truncated extraction artifacts like Hpα (10, 11). Only the mAb 1A12 recognized a band below 3 kDa in all brain extracts in the molecular mass range of RVD-Hpα (1424 Da) (Fig. 2*A*). Additionally, in all extracts, a band at 6 kDa was observed that was most prominent in the AcOH mouse brain extract. In most blots, the lower band stained by the mAb 1A12 appeared relatively broad from ~1.4 to 3 kDa. In comparison, a more discrete band was seen in the blot of the synthetic peptide RVD-Hpα (Fig. 2*B*). To demonstrate specificity, competitive Western blot experiments using increasing concentrations of synthetic RVD-Hpα as competitor were performed. The low molecular weight band seen in the mouse brain extracts was significantly reduced already at a concentration of 3 nM RVD-Hpα, and the band intensity was fully displaced by competitor concentrations above 80 nM (Fig. 2*C*).

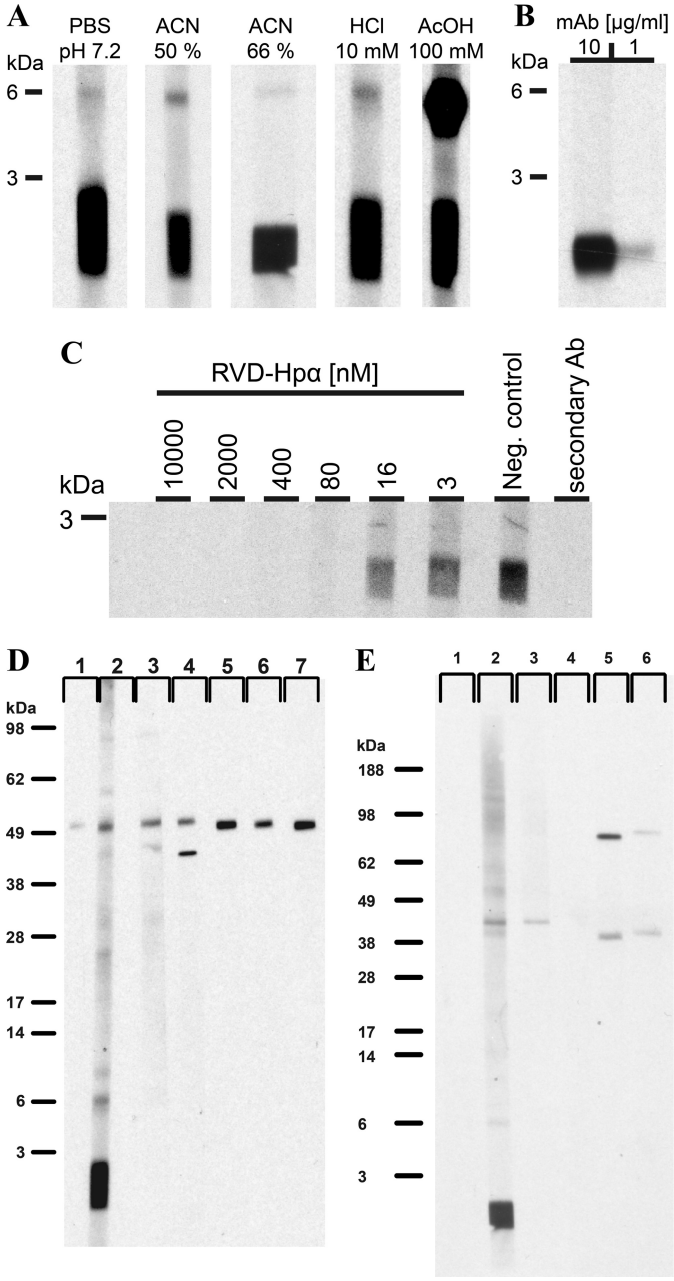

FIGURE 2. *A–C*, Western blots of mouse brain extracts with the mAb 1A12. *A*, Western blots of mouse brain extracts using five different extraction buffers: PBS, pH 7.2, ACN/H_2O 1:1 (ACN 50%), ACN/H_2O 2:1 (ACN 66%), 10 mM HCl, and 100 mM AcOH. *B*, mAb 1A12 recognized the synthetic peptide RVD-Hpα (1423.8 Da) at two different antibody concentrations (10 and 1 μg/ml). *C*, competitive Western blot of the ACN 66% brain extract with the mAb 1A12 using increasing concentrations of the synthetic RVD-Hpα as competitor. 10 μM [Val^5]angiotensin I was taken as negative control peptide. For *A* and *C*, the mAb 1A12 was incubated at 10 μg/ml. Entire Western blots of the 10 mM HCl and ACN 66% mouse brain extracts using six different anti-RVD-Hpα mAbs (1A10 (*lane 1*), 1A12 (*lane 2*), 2C11 (*lane 3*), 7A5 (*lane 4*), 2C1 (*lane 5*), and 8D4 (*lane 6*)) are shown in *D* and *E*, respectively. In both blots, only mAb 1A12 stained a band in the mass range of RVD-Hpα. The 50 kDa band of the HCl extract (*D*) is stained by the secondary antibody (goat anti-mouse IgG γ-chain, *lane 7*). In *blot E*, this band is not visible because ACN efficiently precipitates high molecular weight proteins, such as immunoglobulins. Representative blots of three independent experiments are shown.

Entire Western blots displayed in Fig. 2, *D* and *E*, of an acidic and an ACN extraction, respectively, illustrate the selectivity of the mAb 1A12 for the low molecular weight band.

Identification of N-terminally Extended Peptides by Immunoaffinity MS Experiments—To identify the antigens of the bands stained in Western blots with mouse brain extracts, we performed immunoaffinity MS experiments. A mass spectrum of the mAb 1A12 with mouse brain extract after ACN extraction is shown in Fig. 3*A*. Mass spectra of mouse brains after PBS and acidic extractions showed essentially similar results (Fig. 4). The prominent peak at *m*/*z* 1424.8 represents the singly protonated peptide RVD-Hpα that was identified in all mouse brain extracts independently of the extraction buffer used. Intriguingly, we identified not only RVD-Hpα but also several N-terminally extended peptides, which are listed in Table 3. Additionally, we investigated hamster and rat brain ACN extracts. In hamster brain extracts, we obtained similar results (Fig. 3*B*), whereas in rat brain extracts, no peaks were visible in the corresponding mass range (Fig. 3*C*) possibly because the rat sequence has a Leu → Phe amino acid substitution in the C-terminal part located within the epitope of the mAb 1A12 (Table 2). Reconfirmation of the identification of the peptides by MS/MS fragmentation is representatively shown for the peptides at *m*/*z* 1424.8 and 2011.1 in Fig. 3, *E* and *F*, respectively. The reported brain peptides VD-Hpα and Hpα (8, 10, 12) could not be detected in the extracts despite the fact that, according to our epitope mapping (Fig. 1), the mAb 1A12 was *per se* able to recognize the mouse/human Hpα (PVNFKLLSH) and VD-Hpα (VDPVNFKLLSH) peptides. This is in line with the insight that Hpα is a hot acid extraction artifact (11) and does not occur endogenously. Because RVDPVNFKLLSH together with the newly identified N-terminally extended peptides represents a whole peptide family, and hemopressin is reported to be an artifact and was not found in this study, we propose the new nomenclature Pepcan-X, with X referring to the number of amino acids. Pepcan is the abbreviation for "peptide endocannabinoids" because several identified peptides also showed significant CB_1 receptor binding and functional activities (see below). No peaks corresponding to the 6 kDa band observed in Western blot experiments of brain extracts were found in immunoaffinity MS experiments (data not shown). Apparently, the AcOH extraction was more efficient for Pepcan-17 compared with Pepcan-12, as shown in Fig. 4*C*, which demonstrates the importance of which extraction buffer is used. Several members of the Pepcan family were also identified in mouse (Fig. 3*D*) and human plasma samples (data not shown). Altogether, we identified 11 Pepcans in mouse and hamster brain tissues, and five of them, Pepcan-12, -14, -15, -17, and -20, were also detected in mouse and human plasma (Table 3).

CB_1 Receptor Binding Interactions of Pepcans—Pepcans were investigated for CB_1 receptor binding properties by applying classical radioactivity-based assays and a new fluorescence-based assay. We measured Pepcan-12, -14, -15, -17, and -20, which were detected in rodent brain and mouse/human plasma samples, and the two C-terminally truncated peptides RVD-PVNFKLL and RVDPVNF, which were previously reported to occur in mouse blood (12). First, we carried out conventional radioligand binding assays using [^{3}H]CP55,940 and [^{3}H]WIN55,212-2, which both have low nanomolar affinities toward CB_1 receptors (3, 37). The results showed a weak to moderate radioligand displacement for Pepcan-12, -14, and -20

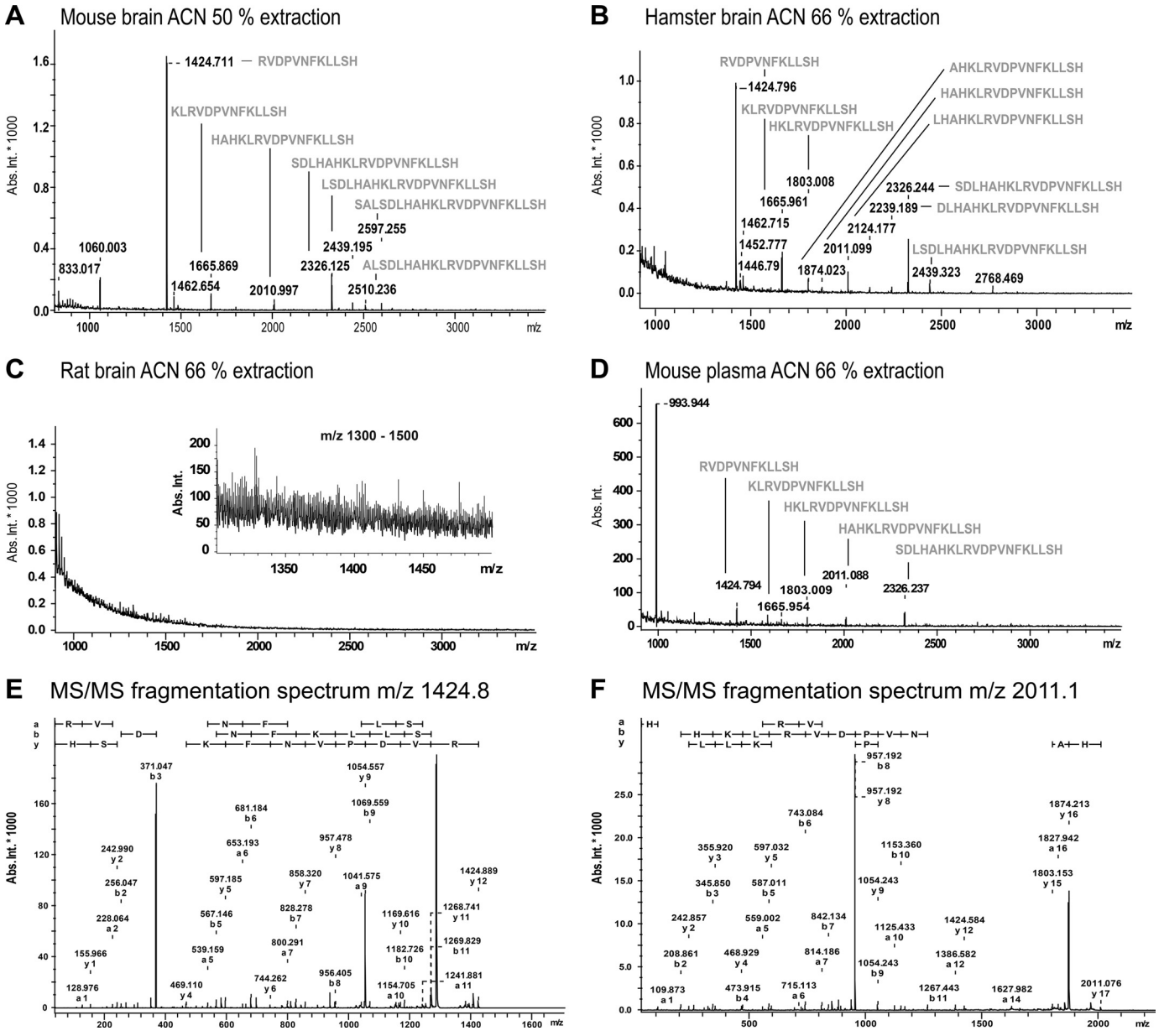

FIGURE 3. **Mass spectra of different rodent brain and a mouse plasma sample extract with immunoaffinity enrichment using the mAb 1A12.** *A–C*, results from mouse, hamster, and rat brains extracted with ACN, respectively. *D*, mass spectrum of mouse plasma extracted with ACN 66%. The identified peptides are displayed in *gray*. *E* and *F*, MS/MS fragmentation spectra of the peaks at *m/z* 1424.8 (RVDPVNFKLLSH) and *m/z* 2011.1 (HAHKLRVDPVNFKLLSH). a-, b-, and y-ion series are displayed in the tandem mass spectra.

at 1 μM, whereas no significant displacement was observed for Pepcan-15 and -17 (Fig. 5, *A* and *B*). Pepcan-12 most efficiently displaced both radioligands by reaching ~50% binding at 1 μM. Therefore, we next characterized Pepcan-12 receptor binding potency toward CB_1 in a concentration-dependent assay. As shown in Fig. 5, *C* and *D*, Pepcan-12 was able to potently but only partially displace both [^{3}H]CP55,940 and [^{3}H]WIN55,212-2. This saturable but incomplete displacement indicated an allosteric rather than a competitive binding interaction. Therefore, we analyzed the Pepcan-12 data with the allosteric TCM model, which is suitable to describe an allosteric interaction between two ligands that bind to topographically distinct binding sites at the same receptor (38). This model has been used previously to confirm the allosteric interaction of the synthetic Organon compounds with the CB_1 receptor (16). Pepcan-12 induced a similar maximal displacement (around 45–50%), of [^{3}H]CP55,940 and [^{3}H]WIN55,212-2 with similar pK_B values. In both cases, the calculated cooperativity constant α was less than 1, indicating a negative allosteric modulation (Table 4). As shown below, Pepcans can form aggregates (dimers or oligomers) at high concentrations (>1 μM); thus, we cannot exclude the possibility that oligomerization may potentially contribute to the partial displacement of the orthosteric ligands. In order to better characterize the allosteric mechanism postulated, we measured the dissociation kinetics of [^{3}H]CP55,940 from CB_1 receptors in the presence of Pepcan-12 or vehicle (39). The experiments were performed using an isotopic dilution approach, where 1 μM

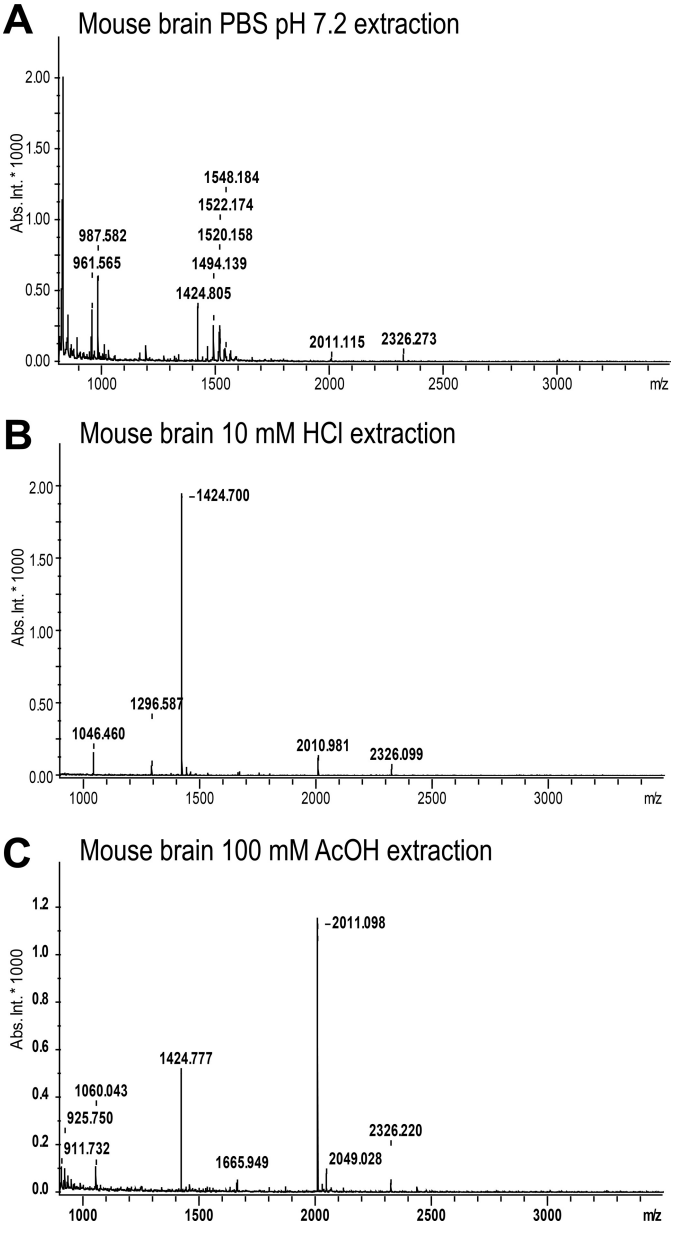

FIGURE 4. **Mass spectra of different mouse brain extracts with immunoaffinity enrichment using mAb 1A12.** *A–C*, spectra from mouse brains extracted with PBS, pH 7.2, 10 mM HCl, and 100 mM AcOH.

TABLE 3

Identified peptides by immunoaffinity MS experiments

Name	Sequence	m/z $[MH^+]^a$	Sample[b]
Pepcan-12 (PC-12)	RVDPVNFKLLSH	1424.8	B + P
Pepcan-14 (PC-14)	KLRVDPVNFKLLSH	1665.9	B + P
Pepcan-15 (PC-15)	HKLRVDPVNFKLLSH	1803.0	B + P
Pepcan-16 (PC-16)	AHKLRVDPVNFKLLSH	1874.0	B
Pepcan-17 (PC-17)	HAHKLRVDPVNFKLLSH	2011.1	B + P
Pepcan-18 (PC-18)	LHAHKLRVDPVNFKLLSH	2124.2	B
Pepcan-19 (PC-19)	DLHAHKLRVDPVNFKLLSH	2239.2	B
Pepcan-20 (PC-20)	SDLHAHKLRVDPVNFKLLSH	2326.3	B+P
Pepcan-21 (PC-21)	LSDLHAHKLRVDPVNFKLLSH	2439.3	B
Pepcan-22 (PC-22)	ALSDLHAHKLRVDPVNFKLLSH	2510.2	B
Pepcan-23 (PC-23)	SALSDLHAHKLRVDPVNFKLLSH	2597.3	B

[a] Measured mass (charge +1) in MALDI-TOF MS experiments.
[b] B, mouse and hamster brain extracts; P, human and mouse plasma extracts.

CP55,940 was added to the CB_1 receptor-bound [^{3}H]CP55,940 in the presence of 300 nM Pepcan-12 or vehicle. As shown in Fig. 5*E*, CP55,940 induced a faster dissociation of the bound [^{3}H]CP55,940 when incubated in the presence of Pepcan-12 compared with vehicle. Data analysis shows higher values of both fast k_1 and slow k_2 dissociation rate constants (Table 5). This enhancement of [^{3}H]CP55,940 dissociation from CB_1 receptors is in line with the partial displacement of the radioligands by Pepcan-12 in the equilibrium binding experiments. Therefore, both results clearly indicate that Pepcan-12 binds to the CB_1 receptor at an allosteric binding site.

With the intention to further characterize the peptide binding site, we generated four fluorescently labeled Pepcan-12 conjugates (Pepcan-F1 to -F4; Table 1). Labeling was done by coupling fluorescein to either the N-terminal or C-terminal part of Pepcan-12 with and without a chemical spacer. The equilibrium binding experiments revealed that N-terminal labeling (with and without spacer) had a negative effect on CB_1 receptor binding properties, whereas C-terminal fluorescein-labeled Pepcan-12 derivatives showed potent receptor binding (Fig. 6*A*). Among all of the derivatives tested, the strongest binding interaction was detected for Pepcan-F4 carrying a C-terminal label, including two aminocaproic acid spacers. We therefore used Pepcan-F4 to further characterize the binding of Pepcans to CB_1 receptors. The apparent K_d value for Pepcan-F4 at human CB_1 receptors (37 ± 0.9 nM) was calculated from concentration-dependent curves (Fig. 6*B*). Additionally, we analyzed the Pepcan-F4 binding selectivity for other receptors activated by endocannabinoids (*i.e.* CB_2, TRPV1, and GPR55). As shown in Fig. 6*C*, Pepcan-F4 showed selective binding to CB_1 and CB_2 receptors but not to GPR55 or TRPV1 receptors. As negative controls, non-transfected CHO cells and $CB_{1/2}$ receptor-negative HL60 cells (27) were used. Pepcan-F4 only stained CB receptor-transfected CHO cells and not non-transfected CHO cells, as illustrated in Fig. 6, *C* and *D*. Intriguingly, staining of cells with Pepcan-F4 occurred immediately, and only one washing step with PBS was necessary to obtain clear images (Fig. 6*D*). The results demonstrate the selectivity of Pepcan-F4 for CB receptors and are in agreement with the results previously published at the functional level for RVDPVNFKLLSH (Pepcan-12) using HEK293 cells stably transfected with CB_1, CB_2, μ-opioid, δ-opioid, α_2-adrenergic, β_2-adrenergic, or AT1 receptors, respectively (9).

We next exploited Pepcan-F4 binding properties to perform competitive displacement experiments in the presence of different concentrations of all Pepcans that we measured *ex vivo*. Pepcan-12, -14, -15, and -17 showed similar CB_1 receptor binding affinities in the nanomolar range (Fig. 7, *A–D*), whereas the longest peptide tested (Pepcan-20) showed no significant Pepcan-F4 displacement up to 10 μM (Fig. 7*E*). We also measured the CB_1 receptor binding affinity of the two C-terminally truncated versions of Pepcan-12 (RVDPVNFKLL and RVDPVNF) that were reported to occur in mouse blood (12). The displacement curves clearly showed only a weak and partial receptor binding to the Pepcan-F4 binding site (Fig. 7, *F* and *G*). In all experiments, the nonspecific binding of Pepcan-F4 was calculated by performing parallel experiments in non-transfected CHO cells. In this case, no synthetic (*i.e.* CP55,940 or WIN55,212-2) or endogenous (*i.e.* AEA or 2-AG) CB_1 receptor ligands could be used to determine the nonspecific binding.

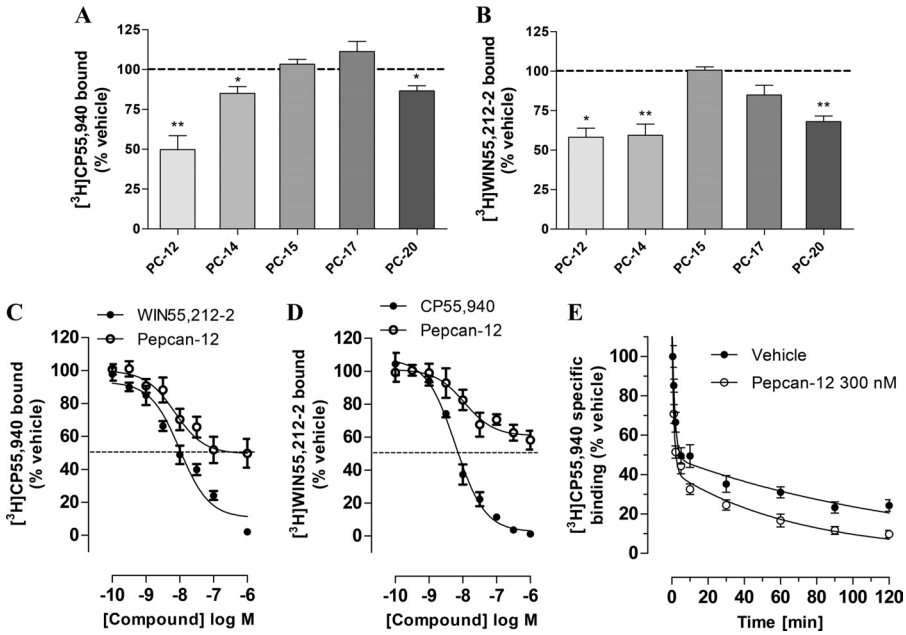

FIGURE 5. *A–D*, Pepcan-induced [^{3}H]CP55,940 and [^{3}H]WIN55,212-2 displacement from human CB_1 receptors. 1 μM Pepcan-12, -14, -15, -17, and -20 was incubated with CHO-*h*CB1 membranes in the presence of 0.5 nM [^{3}H]CP55,940 (*A*) or 2.5 nM [^{3}H]WIN55,212-2 (*B*). Pepcan-12 was the most efficient peptide to displace both radioligands, and therefore its CB_1 binding properties were further investigated. Different concentrations of Pepcan-12 (0.1 nM to 1 μM) were incubated with CHO-*h*CB1 membranes in the presence of 0.5 nM [^{3}H]CP55,940 (*C*) or 2.5 nM [^{3}H]WIN55,212-2 (*D*). The K_i values for the positive controls WIN55,212-2 (2.5 ± 1.3 nM) and CP55,940 (2 ± 1.1 nM) were fitted using the three-parameter one-site competitive binding equation for orthosteric ligands. For Pepcan-12, the allosteric TCM equation was used. The obtained pK_B and α values are shown in Table 3. The nonspecific binding was detected in the presence of 10 μM WIN55,212-2 or CP55,940 for [^{3}H]CP55,940 or [^{3}H]WIN55,212-2, respectively, and subtracted from all data points. Data show means ± S.E. (*error bars*), $n = 12–15$ from 4–5 independent experiments. *, $p < 0.05$; **, $p < 0.01$, one-way analysis of variance followed by Dunnett's post hoc test. *E*, dissociation of 0.5 nM [^{3}H]CP55,940 from human CB_1 receptors in presence of 1 μM CP55,940 plus either vehicle or 300 nM Pepcan-12. The data were analyzed by a two-phase exponential decay model and the obtained rate constants, and corresponding half-lives of both phases are listed in Table 4. Results show means ± S.E. ($n = 15$) from five independent experiments. The corresponding equations for all models mentioned are given under "Experimental procedures."

TABLE 4

Allosteric TCM binding parameters (see "Experimental Procedures" for descriptions) for Pepcan-12 at *h*CB_1 receptors

pK_B is the negative logarithm of the equilibrium dissociation constant of the allosteric modulator Pepcan-12, and α is the cooperativity factor. Results for pK_B are shown ± S.E. and for α with its 95% confidence interval range in parentheses.

Radioligand + parameter	Allosteric modulator (Pepcan-12)
[^{3}H]CP55,940	
pK_B	8.33 ± 0.26
α	0.33 (0.25–0.43)
[^{3}H]WIN55,212–2	
pK_B	8.09 ± 0.25
α	0.43 (0.35–0.53)

We further measured the effects of the endocannabinoids AEA and 2-AG and the synthetic high affinity ligands CP55,940, SR141716A, and WIN55,212-2 on Pepcan-F4 binding to CB_1 receptors (Fig. 7, *H–K*). Based on fluorescence, AEA and 2-AG increased Pepcan-F4 binding to CB_1 receptors only at the highest concentration tested (10 μM) (Fig. 7*H*), whereas SR141716 significantly increased the fluorescence signal already at 1 μM (Fig. 7*I*). The two high affinity CB receptor ligands CP55,940 and WIN55,212-2 differed in their effects. CP55,940 was ineffective (Fig. 7*J*), whereas WIN55,212-2 induced a strong concentration-dependent increase in fluorescence intensity (Fig. 7*K*). Altogether, these results suggest an allosteric modulation of Pepcan-F4 to orthosteric cannabinoid ligands rather than a competitive interaction on the same binding site.

Quantification of Pepcans by Competitive ELISA—According to the results of the binding experiments, not only Pepcan-12 but also Pepcan-14, -15, and -17 strongly bound to CB receptors (K_i values of 2–29 nM). Thus, although Pepcan-12 may be the major peptide endocannabinoid in the brain, the other Pepcans could also play a physiological role. To estimate the absolute levels of Pepcans in mouse brain tissue and human plasma samples, we developed a C-ELISA for their quantification. In a first step, the relative affinity of four mAbs toward the synthetic Pepcan-12 was determined using Pepcan-12 as competitor for the binding of the mAbs toward a coated ovalbumin-peptide conjugate (Table 1). The pIC_{50} values of the mAbs are listed in Table 2. The mAb 1A12, which already showed the best results in Western blot and immunoaffinity MS experiments, also had the highest affinity toward Pepcan-12 in C-ELISA experiments and was therefore chosen for establishing the quantification assay.

The $\alpha_2\beta_2$ tetramer hemoglobin (Hb) was reported to dissociate into $\alpha\beta$ dimers or even further into monomers when released from red blood cells (40, 41), potentially uncovering parts of the epitope of the Pepcan-12 sequence in the protein (Fig. 8, *A* and *C*). We therefore investigated whether Hb interferes in the C-ELISA. The results demonstrated that interference is only seen at very high Hb concentrations; interference was seen above 2 μM (130 ng/ml) without extraction and above 20 μM (1.3 mg/ml) and 50 μM (3.3 mg/ml) after ACN 50% and ACN 66% extractions, respectively. BSA did not have any effect on the pIC_{50} of Pepcan-12 at different concentrations (Table 6), indicating that the decrease in signal intensity by Hb was probably of a specific nature and not just caused by increasing protein concentration.

TABLE 5

Dissocation rate constants for [^{3}H]CP55,940 at *h*CB_1 receptors in the presence and absence of the allosteric modulator Pepcan-12, respectively

An extra-sum-of-squares test (F test, $p < 0.001$) significantly revealed that the exponential decay was biphasic compared with a corresponding one-phase model. Results for the fast (k_1) and the slow (k_2) slow dissociation rate constants are shown ± S.E. and for half-life values with their 95% confidence interval range in parentheses.

	k_1 (fast)	Half-life (fast)	k_2 (slow)	Half-life (slow)
	min^{-1}	*min*	$\times 10^{-2}\ min^{-1}$	*min*
Vehicle	0.67 ± 0.18	1.03 (0.67–2.24)	0.72 ± 0.14	96.2 (69.14–158.0)
Pepcan-12 (300 nM)	0.84 ± 0.32	0.82 (0.47–3.46)	1.46 ± 0.23[a]	47.6 (36.0–70.0)

[a] $p < 0.05$, Student's unpaired *t* test.

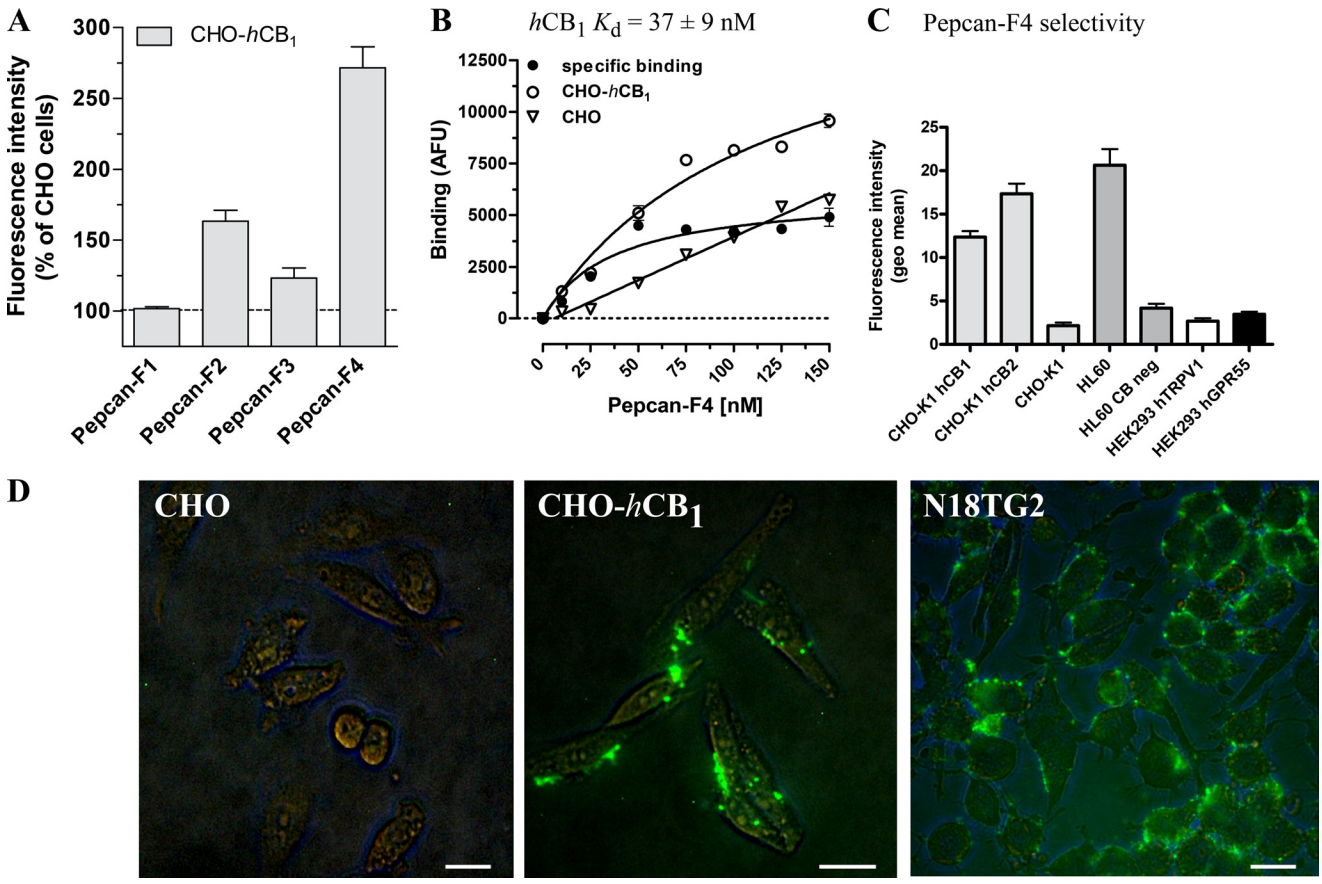

FIGURE 6. **Pepcan-F4 receptor binding properties and selectivity studies.** *A*, 100 nM of each of the fluorescein-labeled Pepcan-12 derivatives, Pepcan-F1 to -F4 (Table 1), was incubated with 1×10^5 CHO-*h*CB_1 cells for 60 min at 37 °C and then washed twice with ice-cold binding buffer. Fluorescence intensities were compared with non-transfected CHO cells. Data show means ± S.E. (*error bars*) ($n = 6$) from two independent experiments. *B*, total, nonspecific, and specific saturation binding curves of Pepcan-F4. The K_d value was obtained by nonlinear fit (one-site specific binding model) of the specific binding curve, which was obtained by subtracting the fluorescence intensity measured in untransfected CHO cells (nonspecific binding) of the fluorescent signal measured in CHO-*h*CB1 cells (total binding). Data show means ± S.E. ($n = 6$) from three independent experiments. *AFU*, arbitrary fluorescence units. *C*, binding interactions of Pepcan-F4 with different human receptor (CB_1, CB_2, $TRPV_1$ and GPR55)-transfected and untransfected cell lines. A 250 nM concentration of Pepcan-F4 was incubated with 2×10^6 detached cells for 60 min at 37 °C under shaking and washed twice with PBS, 0.5% BSA, 5% FCS prior to measurement by FACS on a FACScan BD equipped with a solid state laser (Cytek). Data were analyzed on the CellQuest software. FACS experiments were carried out as described before (72). The CB receptor-negative HL60 cell line was described previously (72). Data show mean fluorescence values (*geo mean*) ± S.D. ($n = 9$) from three independent experiments. *D*, representative images of three independent experiments of wild-type CHO, CHO-*h*CB_1, and N18TG2 cells with Pepcan-F4 (100 nM for CHO and CHO-*h*CB_1 cells; 1 μM for N18TG2). Cells were incubated for 60 min at 37 °C and washed once with PBS. Images were obtained with a Nikon DSFi1 camera mounted on a Nikon Eclipse TS100 microscope equipped with a Tripleband DAPI/FITC/TRITC HC filter set (AHF, Tübingen, Germany). *Bar*, 10 μm.

For the subsequent quantification, we decided to use the ACN 66% extraction, which was found to be equally efficient for Pepcans of different length (Table 6 and Fig. 9*C*). Furthermore, ACN nonspecifically precipitates protein, including Hb, and can be easily evaporated, eliminating an additional neutralization step that would be mandatory after an acidic extraction.

All Pepcans tested showed similar affinity to the mAb 1A12 after ACN extraction (pIC_{50} values from 8 to 8.3), whereas the C-terminally truncated peptides had much lower affinity (Fig. 9, *B* and *C*, and Table 6), thus confirming the epitope mapping results. Because VD-Hpβ (VDPENFRLLGNM) of the Hb β chain was also reported to occur in mouse brain extracts (10) and closely resembles the Pepcan-12 sequence (RVDPVNFKLLSH), we performed experiments with the most analogous synthetic Hb β chain peptide HVDPENFRLLGN and observed a very low binding affinity ($pIC_{50} = 4.79 \pm 0.04$; Fig. 9*B*). The linearity of the quantification assay was evaluated by analysis of 11 calibrators using a four-parameter logistic nonlinear regression model to fit the response (42, 43). A representative stan-

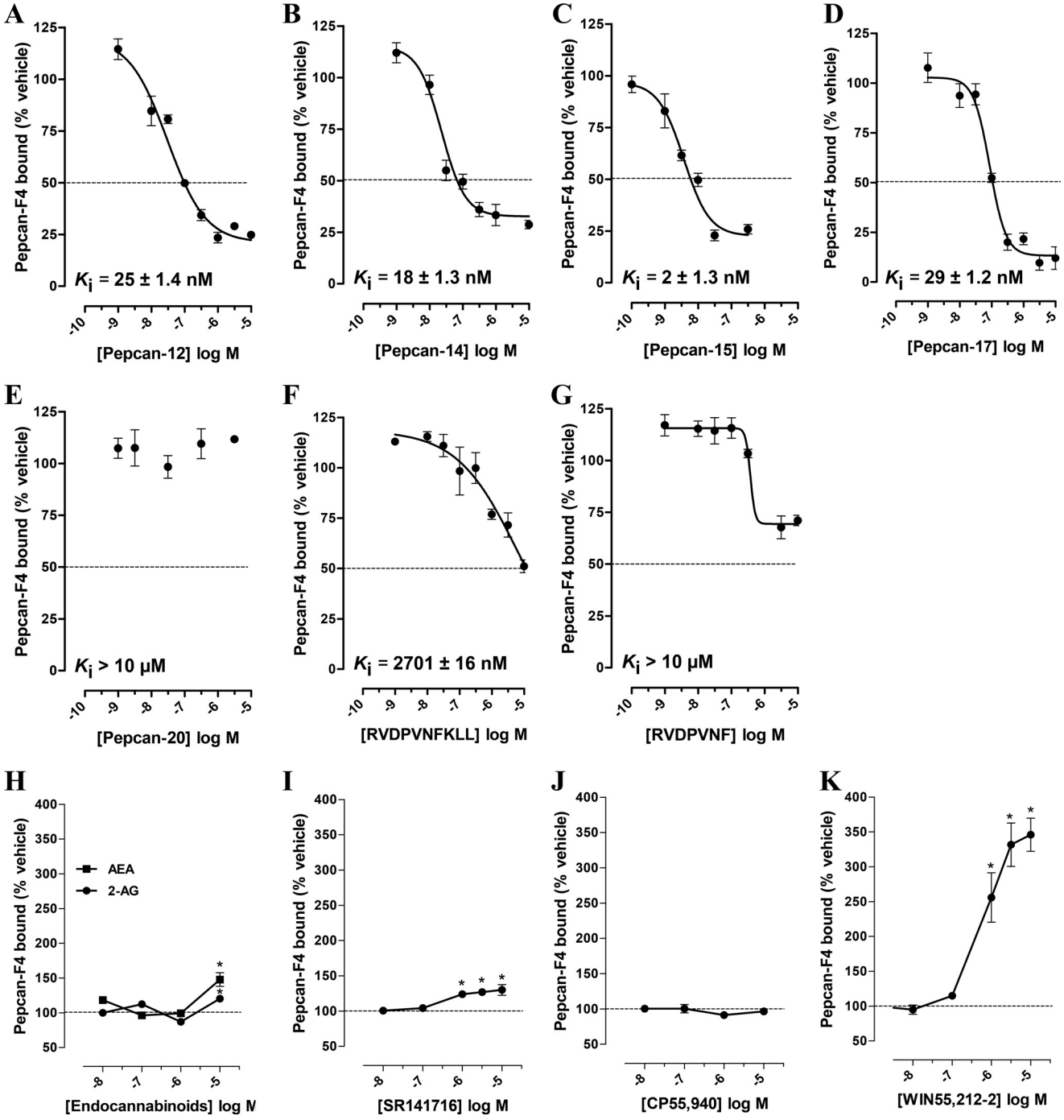

FIGURE 7. **Pepcan-induced Pepcan-F4 displacement from human CB_1 receptors.** Different concentrations (1 nM to 10 µM) of Pepcan-12 (*A*), -14 (*B*), -15 (*C*), -17 (D), -20 (*E*), RVDPVNFKLL (*F*), and RVDPVNF (*G*) were incubated with 1 × 10^6 CHO-*h*CB1 cells in the presence of a 100 nM concentration of the fluorescently labeled Pepcan-F4 for 60 min at 37 °C under shaking. The IC_{50} values ("absolute" IC_{50} values representing the concentration of competitor displacing 50% of Pepcan-F4 (33)) of Pepcans were estimated from fitted nonlinear curves and were used to calculate the K_i values by applying the Cheng-Prusoff equation as described under "Experimental Procedures." Data show means ± S.E. (*error bars*) (n = 6–9) from 2–3 independent experiments. 1 × 10^6 CHO-*h*CB1 cells were incubated with 100 nM Pepcan-F4 in the presence of different concentrations of AEA or 2-AG (*H*), SR141716 (*I*), CP55,940 (*J*), and WIN55,212-2 (*K*) for 60 min at 37 °C under shaking. 2-AG and AEA weakly increased the Pepcan-F4 fluorescence intensity only at 10 µM, whereas SR141716 and WIN55,212-2 (1 and 10 µM) induced a moderate and high fluorescence increase, respectively (*, $p < 0.05$, Student's unpaired *t* test of competitor *versus* vehicle control). Data show means ± S.E. (n = 6–9) from 2–3 independent experiments.

dard curve of Pepcan-12 after ACN 66% extraction is shown in Fig. 9*D*. In order to determine the endogenous amounts of peptides in mouse brain and human plasma, we performed spike and recovery experiments in both matrices. The results are shown in Table 7 together with the quantification results of Pepcans in physiological samples. The recoveries varied from 73 to 98% in the relevant concentration range for mouse brain samples and from 44 to 100% for human plasma samples.

The average endogenous amount of quantified Pepcans in three mouse brains was 92 ± 7 pmol/g brain tissue (22.7 ± 1.7 nM in C-ELISA). The average endogenous concentration of Pepcans in human plasma of four healthy volunteers (three

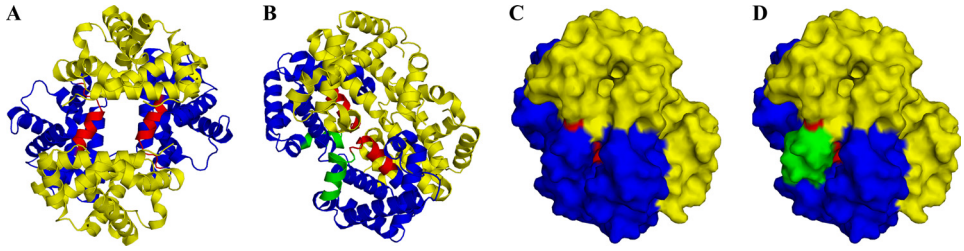

FIGURE 8. **Structural representations of the $\alpha_2\beta_2$ tetramer Hb (Protein Data Bank entry 2DN2) that display the location of the α-chain-derived Pepcan-12 (RVDPVNFKLLSH) sequence (colored in *red*) until Pepcan-23 (SALSDLHAHKLRVDPVNFKLLSH) with the sequence SALSDLHAHKL colored in *green*.** *A* and *B*, images of Hb with Hb α-chains *colored* in *blue* and β-chains in *yellow*. *C* and *D*, surface plots of Hb show the internal location of Pepcan-12 and demonstrate that the N-terminal part of Pepcan-23 reaches the protein surface, possibly exposing it for a proteolytic attack. Images were generated using PyMOL software.

TABLE 6

Displacement of the binding of the mAb 1A12 toward a synthetic ovalbumin-Pepcan-12 conjugate (Table 1) by selected competitors

pIC_{50} values were estimated using nonlinear regression (shared E_{max} values in *A* and *B* assuming curves would reach maximal displacement at higher concentrations).

	Extraction method	
	No extraction	ACN 66%
Hemoglobin	4.45 ± 0.01	3.61 ± 0.04
PC-12	8.02 ± 0.02[a]	8.0 ± 0.03[b]
PC-14	8.25 ± 0.02	8.23 ± 0.01
PC-15	8.4 ± 0.03	8.2 ± 0.02
PC-17	8.36 ± 0.01	8.17 ± 0.01
PC-20	8.42 ± 0.02	8.28 ± 0.02
PVNFKFLSH	7.26 ± 0.05	6.85 ± 0.02
RVDPVNFKLL	6.15 ± 0.05	5.82 ± 0.02
RVDPVNF	<4	<4
HVDPENFRLLGN	4.87 ± 0.08	4.79 ± 0.04
[Val^5]Angiotensin I	<4	<4
PC-12 + 3.5 mg/ml BSA	8.11 ± 0.02	
PC-12 + 5 mg/ml BSA	8.08 ± 0.02	
PC-12 + 7.5 mg/ml BSA	8.12 ± 0.01	
PC-12 + 12.5 mg/ml BSA	8.13 ± 0.02	

[a] Averaged value from $n = 8$ in four independent experiments.
[b] Averaged value from $n = 6$ in three independent experiments.

female and one male) was 6.3 ± 2.3 nM. Therefore, the determined nanomolar binding interactions of Pepcans with CB_1 receptors correspond well to the nanomolar concentrations of Pepcans quantified in mouse brain tissue and human plasma samples.

Pepcans Act as Negative Allosteric Modulators of Cannabinoid Signaling at CB_1 Receptors—Because several conformational states are known for G protein-coupled receptors, allosteric modulators have been discovered which affect orthosteric ligand efficacy, in addition to or independently of effects on ligand affinity (16, 39, 44–47). Thus, we next investigated the effects of Pepcans on the efficacy of orthosteric ligands at the CB_1 receptor in different functional assays.

First, we established an assay measuring cAMP accumulation in the same cell system as used for CB_1 receptor binding. We transfected CHO-*h*CB_1 and wild-type CHO cells with the plasmid pGloSensor-22F of the GloSensor™ luminescence assay (Promega) for detecting cAMP levels in living cells. The assay was validated by using CP55,940, WIN55,212-2, and 2-AG as agonists and SR141716 as inverse agonist (Fig. 10*A*). Surprisingly, we observed an increase of basal cAMP levels after agonist stimulation and a decrease after inverse agonist stimulation in line with a G_s response of the CB_1 receptor, whereas in the literature, the most common reported response is mediated by $G_{i/o}$. Whereas CB_1 receptor agonists were shown to inhibit forskolin-stimulated adenylyl cyclase by activation of pertussis toxin (PTX)-sensitive $G_{i/o}$ proteins (48–51), they have also been shown to positively couple to adenylyl cyclase via PTX-insensitive G_s proteins with or without forskolin stimulation (52–55). We were able to measure cAMP accumulation upon agonist stimulation without forskolin stimulation and also without significant inhibition of the $G_{i/o}$ signaling pathway by PTX (Fig. 10*B*). This putative G_s-mediated pathway of the CB_1 receptor is in agreement with the literature, where a PTX-insensitive adenylyl cyclase stimulatory pathway upon agonist exposure without forskolin stimulation has been also shown (54, 56). The synthetic cannabinoid WIN55,212-2 and the endocannabinoid 2-AG acted as full agonists in comparison with CP55,940 (Fig. 10*A* and Table 8), which is in line with a previous report (55). Importantly, SR141716 efficiently decreased basal cAMP levels down to 14% (Fig. 10*A*). Pepcan-12 did not elicit any changes in basal cAMP levels up to 1 μM (Fig. 10*A*). None of the tested compounds showed any change in basal cAMP levels in the wild-type CHO cells, indicating a strictly CB_1-receptor mediated cAMP accumulation in the CHO-*h*CB_1 cells. Next, we decided to investigate whether Pepcan-12 would exert negative or positive allosteric effects on the efficacy and/or potency of cAMP accumulation induced by the orthosteric ligands. Because the extent and direction of an allosteric interaction can vary between different orthosteric ligands due to the so-called "probe dependence" (38, 57), we chose two distinctly different orthosteric ligands for the interaction studies: 2-AG, representing the most abundant endogenous CB_1 receptor agonist in brain tissue, and the synthetic agonist WIN55,212-2. Pepcan-12 concentration-dependently reduced the efficacy of cAMP accumulation induced by both WIN55,212-2 and 2-AG without significantly affecting the potency (Fig. 10, *C* and *F*, and Table 8). Pepcan-12 was able to reduce the maximal efficacy (E_{max}) of these cannabinoids from 20–30% at 1 nM up to 45–47% at 1 μM. The same experiments were also conducted in the presence of different concentrations of the inverse agonist SR141716 (Fig. 10, *D* and *G*). Unlike Pepcan-12, SR141716 did not affect the efficacy of orthosteric agonists but concentration-dependently decreased their potency represented by decreasing pEC_{50} values (Table 8). The interaction of different SR141716 concentrations on WIN55,212-2-induced cAMP accumulation was analyzed using a Schild plot (see "Experimental Procedures" and Fig. 10*E*), where competitive and non-competitive ligands can be distinguished. The slope near unity (1.19 ± 0.12) clearly indicates competitive interaction of SR141716 with WIN55,212-2, and also the calcu-

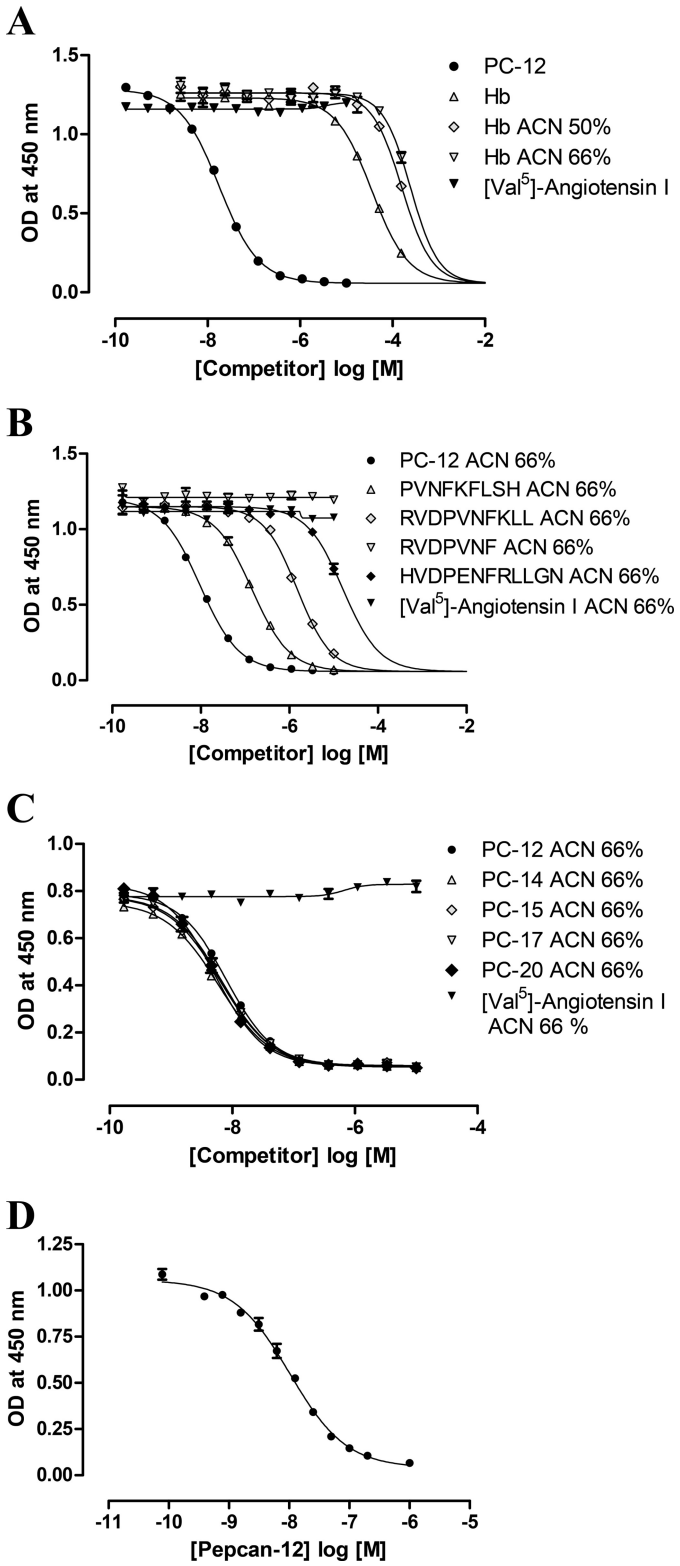

FIGURE 9. **Characterization of the mAb 1A12 in C-ELISA.** Selected compounds were analyzed for their potential to displace the binding of the mAb 1A12 toward the coated ovalbumin-Pepcan-12 conjugate (Table 1) in C-ELISA with or without ACN extraction. *A*, Hb with and without ACN extractions. *B*, rat hemopressin (PVNFKFLSH), the C-terminal truncated peptides RVDPVNFKLL and RVDPVNF, and the hemoglobin β-chain-derived peptide HVDPENFRLLGN after ACN extraction. *C*, Pepcan-14, -15, -17, and -20 after ACN extraction. As a reference peptide, Pepcan-12 was used, and the similar sized peptide [Val^5]angiotensin I served as negative control. *D*, representative standard curve of the synthetic Pepcan-12 used for the quantification of Pepcans from mouse brain and human plasma. pIC_{50} values of compounds with and without ACN extractions were obtained from nonlinear regression (shared bottom values for *graphs A* and *B*) and are listed in Table 6. The corresponding graphs for peptide competitors without ACN extraction are not shown because the pIC_{50} values did not differ substantially from the ones obtained with ACN extraction. Data show means ± S.D. (*error bars*) ($n = 2–3$) in *A–C* and a cumulated standard curve of two independent experiments in duplicates in *D*.

lated K_d value of 2.5 nM derived from the *x* intercept at $y = 0$ is in accordance with literature (3, 58). In summary, the Pepcan-12-induced decrease of efficacy and concomitant lack of a right shift of the WIN55,212-2 and 2-AG cAMP accumulation curves indicate a negative allosteric modulation of the orthosteric binding site, thus confirming the receptor binding data. Importantly, with both ligands, the same effects were obtained, and therefore no "probe dependence" was observed.

The next step in our study was the confirmation of these results in a more physiological system as both experiments, the receptor binding as well as the cAMP accumulation assay, were performed using recombinant cells with artificially high expression of CB_1 receptors. Therefore, we performed [^{35}S]GTPγS binding assays using mouse cerebellar membranes in which a CB_1 receptor-dependent $G_{i/o}$ signaling response is known to be prevalent (51, 59). The species difference in this case was irrelevant because the mouse and human sequence of Pepcan-12 are identical. Intriguingly, we observed the same negative allosteric modulation seen with Pepcan-12 on HU-210-induced [^{35}S]GTPγS binding (Figs. 10, *H* and *I*). Pepcan-12 was ineffective by itself in changing basal [^{35}S]GTPγS binding but significantly decreased by 20% the maximal efficacy of HU-210 without affecting potency, which is in good agreement with its allosteric binding. SR141716 was used to demonstrate the distinctly different behavior between the non-competitive allosteric modulator Pepcan-12 and the competitive inverse agonist at the orthosteric binding site. As shown, SR141716 induced a decreased potency of HU-210 without altering its efficacy (Fig. 10*I* and Table 8). It is noteworthy that in both cAMP accumulation and [^{35}S]GTPγS binding assays, all responses induced by agonists could be fully inhibited by higher concentrations of SR141716, thus demonstrating the CB_1 receptor specificity for the observed responses (Fig. 10, *D*, *G*, and *I*). For [^{35}S]GTPγS binding using 2-AG, the effect plateau was not achieved up to 50 μM, probably due to a strong and multienzymatic 2-AG degradation present in the cerebellar preparation, despite the pretreatment with the serine hydrolase inhibitor PMSF. However, Pepcan-12 almost completely abolished [^{35}S]GTPγS binding induced by 80 nM 2-AG to basal levels and significantly reduced the effects induced by 10 and 50 μM 2-AG (Fig. 10*J* and Table 8).

In order to profile the other Pepcans in cAMP accumulation and [^{35}S]GTPγS binding assays, we incubated 1 and 100 nM concentrations of the Pepcans with the same CB_1 receptor agonists used for Pepcan-12 interaction studies. The concentrations of the agonists were chosen at maximal response, and the impact of Pepcans on the efficacy was investigated. As shown in Fig. 11, *A* and *B*, Pepcan-12 was still the most efficient negative allosteric modulator, but Pepcan-14, -17, and -20 also showed a significant partial inhibition, especially of 2-AG signaling. It is noteworthy that, although a dose-response was observed in

TABLE 7
Results of spike and recovery experiments and quantification results for mouse brain and human plasma samples

	Spike	Statistics				Sample	Results ± S.D.
		Mean	S.D.	CV[a]	Recovery[b]		
	nM			%	%		nM
Brain	0	16.9	1.1	6.3			
	12.5	29.1	10.1	34.7	98.2	NMRI mouse brain 1[c]	26.1 ± 1.28[d]
	25	35.0	3.6	10.1	72.6	NMRI mouse brain 2	18.3 ± 2.6[d]
	100	56.2	7.6	13.4	39.4	NMRI mouse brain 3	23.6 ± 1.3[d]
Plasma	0	<LLOQ[e]					<LLOQ
	0.78	1.11	0.19	17.7	143.1	Human plasma, female 1	1.31 ± 0.67[f]
	1.56	1.56	0.39	25.1	100.1	Human plasma, female 2	6.23 ± 0.65[f]
	12.5	5.5	0.6	10.6	43.6	Human plasma, female 3	5.05 ± 2.1[f]
	25	14.4	2.4	16.3	57.8	Human plasma, male 1	<LLOQ[f]
	100	50.9	4.7	9.3	50.9		

[a] Coefficient of variation.
[b] Percentage recovery was calculated by subtracting the endogenous amount (spike 0 nM) from the measured value, divided by the nominal spike value multiplied by 100. For plasma samples, no endogenous amount could be subtracted because it was below the lower limit of quantification (~1 nM).
[c] NMRI mouse brains 1, 2, and 3 = 0.49, 0.49, and 0.50 g wet weight, respectively.
[d] These values correspond to 107 ± 5 pmol of Pepcans/g of mouse brain, 75 ± 11 pmol of Pepcans/g of mouse brain, and 94 ± 5 pmol of Pepcans/g of mouse brain (calculated for 1:1 diluted samples and 1 ml of total brain extract).
[e] LLOQ, lower limit of quantification.
[f] These values correspond to 2.6 ± 1.3, 12.5 ± 1.3, and 10.1 ± 4.2 nM (calculated from the values obtained for 1:1 diluted samples in the competitive ELISA). For the calculation of the average endogenous amounts of Pepcans in plasma, we adapted a concentration of 0 nM for the male sample.

cAMP accumulation experiments using CHO-*h*CB_1 cells, no dose response could be achieved in [^{35}S]GTPγS binding assays in mouse cerebellar homogenates. We assume that differences in the cell preparation (living cells *versus* homogenates) and the incubation times (3 min at 30–37 °C in the cAMP assay *versus* 60 min at 37 °C in the [^{35}S]GTPγS binding assay) play a role in Pepcan aggregation. In order to experimentally address the aggregation phenomenon, we used an ultrafiltration approach combined with a subsequent quantification of Pepcans by C-ELISA to estimate the degree of peptide aggregation at low and physiological concentrations. As shown in Fig. 11*C*, by using ultrafiltration tubes with a molecular weight cut-off of 2000, Pepcan-12 and -20 showed a significant loss of recovery (~40%) at 1 μM concentration after 1 h of incubation at 37 °C relative to 10 nM concentrations. This indicates that aggregation occurs in a peptide concentration-dependent manner. On the contrary, when we used ultrafiltration tubes with a molecular weight cut-off of 3000, the recovery was almost fully restored. This difference suggests that at high concentrations, Pepcans form lower molecular weight aggregates, such as dimers or trimers.

Finally, we addressed the question whether Pepcans can also activate CB_1 receptor as reported before for Pepcan-12 (RVD-Hpα) (10). Pepcan-12 was reported to induce internalization of the CB_1 receptor in CHO cells expressing *myc*-tagged CB_1 receptors (10). Thus, we assessed the effects of Pepcans on CB_1 receptor internalization/externalization in CHO-*h*CB_1 cells using the FACS-based method reported previously (31). As shown in Fig. 11*D*, at 1 μM, Pepcan-12 induced the strongest receptor internalization (21%), followed by Pepcan-14 (20%), Pepcan-15 (12%), Pepcan-17 (10%), and Pepcan-20 (7%), thus confirming the results in the literature (10). As positive controls, we used the agonists WIN55,212-2 (36% internalized receptors) and 2-AG (22% internalized receptors) and the inverse agonist (antagonist) SR141716 (15% externalized receptors). Intriguingly, when WIN55,212-2 and 2-AG were co-incubated with Pepcan-12, the latter exerted an antagonistic effect by partially reversing the CB_1 receptor internalization induced by the CB_1 receptor agonists. No significant effects were observed when Pepcan-12 was co-incubated with SR141617. Altogether, these data support the negative allosteric mechanism of Pepcan-12 at CB_1 receptors. To ensure that Pepcan-12 does not indirectly affect CB_1 receptors through modulation of AEA and 2-AG levels, we measured the effect of Pepcan-12 on AEA and 2-AG hydrolysis in pig brain homogenates, as previously described (28). As shown in Fig. 12, Pepcan-12 did not affect AEA and 2-AG degradation up to 10 μM.

DISCUSSION

Identification of Pepcans in Brain and Plasma Samples Using High Affinity mAbs—The previous report on potentially endogenous peptide agonists for the CB_1 cannabinoid receptor (10) motivated us to raise mAbs against the peptide RVDPVNFKLLSH. Because we failed to generate suitable mAbs against the highly conserved peptide sequence in a conventional mouse strain (data not shown), we decided to use the autoimmune-prone (NZB×NZW)F1 hybrid mouse strain. We were able to generate mAbs recognizing C-terminal epitopes and neo-epitopes of the peptide RVDPVNFKLLSH, the sequence of which is buried in its source protein Hb (Fig. 8, *A* and *C*). The mAb 1A12 recognized the synthetic peptide as well as a broader band in the same molecular weight range in different mouse brain extracts in Western blot experiments. The extended molecular weight range of these bands was due to the fact that the mAb recognized, in addition to RVDPVNFKLLSH, several N-terminally extended peptides from 1.4 to 2.6 kDa, as demonstrated by immunoaffinity MS experiments. Because hemopressin is not found endogenously using the mAbs and the soft extraction protocols (*i.e.* it is an extraction artifact), the newly identified peptides together with RVDPVNFKLLSH (Pepcan-12) were designated Pepcans (peptide endocannabinoids). The term "peptide endocannabinoids" was already mentioned previously by Gomes *et al.* (10). In immunoaffinity MS experiments, we could not detect a peak corresponding to the 6 kDa band observed in Western blots of mouse brain extracts, suggesting either that these antigens are only generated in the Western blot experiments or that they have reduced affinity to the mAbs and that binding interactions are lost during the

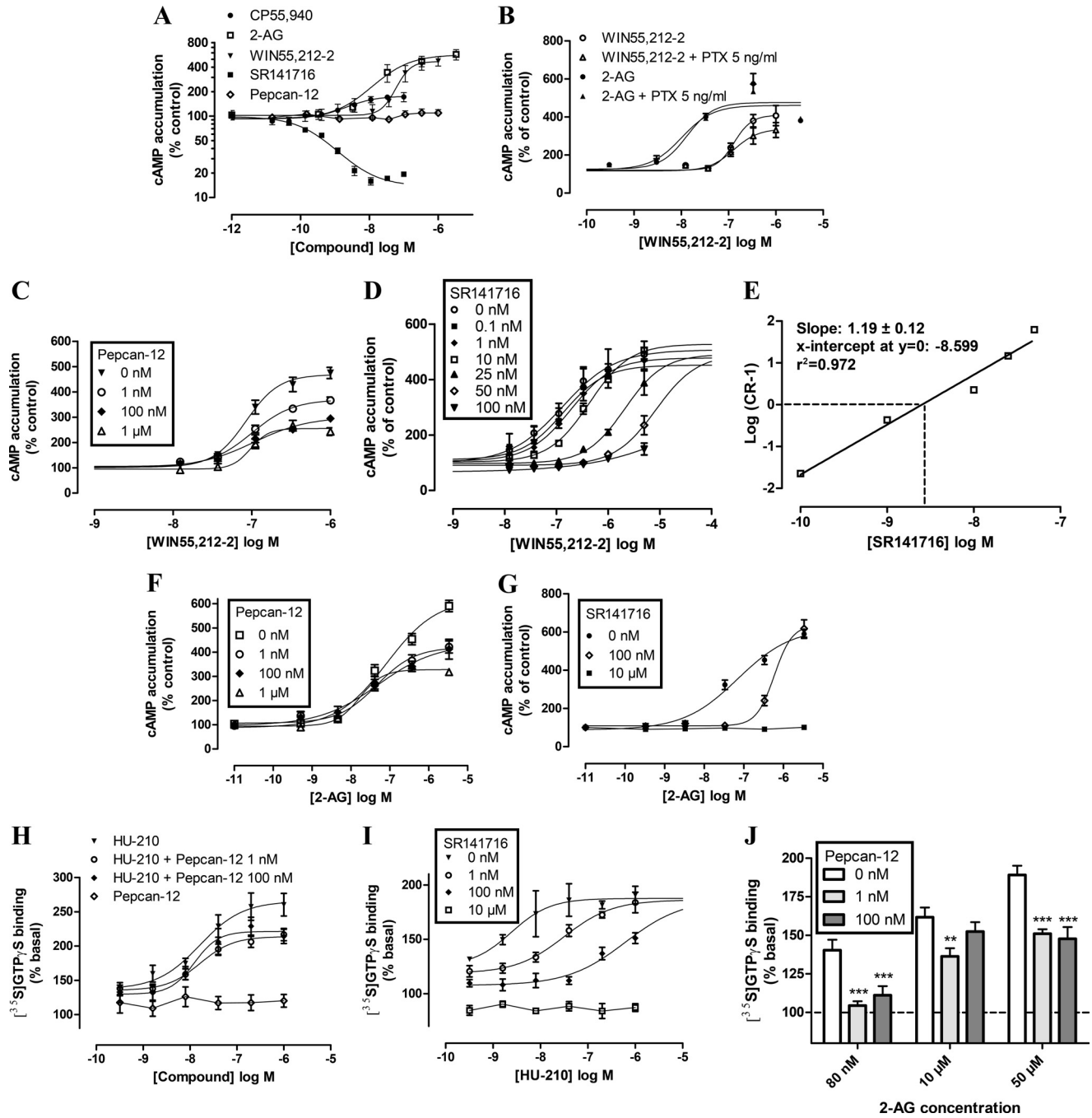

FIGURE 10. **Negative allosteric modulation of cannabinoid signaling at the human CB_1 receptor by Pepcan-12.** All data were analyzed by using a four-parameter dose-response model with variable slope described under "Experimental Procedures." *A*, measurement of cAMP accumulation induced by CP55,940 ($pEC_{50} = 8.55 \pm 0.15$ nM; $E_{max} = 176.5 \pm 8.0$), WIN55,212 (see Table 8), 2-AG (see Table 8), SR141716 ($pEC_{50} = 9.48 \pm 0.08$ nM; $E_{max} = 13.7 \pm 2.87$), and Pepcan-12 (no significant change of basal cAMP accumulation) at hCB_1 receptors. Results show means ± S.E. (*error bars*) ($n = 6–15$) from 2–5 independent experiments. *B*, preincubation for 16 h with 5 ng/ml PTX did not significantly alter the cAMP accumulations induced by WIN55,212-2 and 2-AG. Data show means ± S.D. ($n = 4$) of two independent experiments. *C* and *D*, WIN55,212-2-stimulated cAMP accumulation in the presence of different concentrations of Pepcan-12 (*C*) and SR141716 (*D*) (0 nM (vehicle control): $pEC_{50} = 6.88 \pm 0.15$, $E_{max} = 506.7 \pm 36.6$; 0.1 nM: $pEC_{50} = 6.87 \pm 0.22$, $E_{max} = 452.0 \pm 66.8$; 1 nM: $pEC_{50} = 6.72 \pm 0.10$, $E_{max} = 477.9 \pm 28.1$; 10 nM: $pEC_{50} = 6.36 \pm 0.09$*, $E_{max} = 527.7 \pm 35.7$; 25 nM: $pEC_{50} = 5.68 \pm 0.05$***, 50 nM: $pEC_{50} = 5.08 \pm 0.09$***. E_{max} values for the nonlinear fits of the 25 and 50 nM curves were constrained to 491.1, representing the average E_{max} values of the other curves. *, $p < 0.05$; ***, $p < 0.001$, one-way analysis of variance followed by Dunnett's post hoc test). Data show means ± S.E. ($n = 9$) from three independent experiments. Results from *D* were used to generate a Schild plot (*E*) (see "Experimental Procedures") for the analysis of competitive binding of SR141716. Shown is 2-AG-stimulated cAMP accumulation in the presence of different concentrations of Pepcan-12 (*F*) and SR141716 (*G*). Data show means ± S.E. ($n = 6–9$) from 2–3 independent experiments. Shown is HU-210-stimulated [^{35}S]GTPγS binding in the presence of different concentrations of Pepcan-12 (*H*) and SR141716 (*I*). Pepcan-12 did not elicit a significant change of basal [^{35}S]GTPγS binding. Results show means ± S.E. ($n = 6–30$) from 2–10 independent experiments. pEC_{50} and E_{max} values of the curves displayed in *C* and *F–I* are shown in Table 8. *J*, partial reduction of the [^{35}S]GTPγS binding by Pepcan-12 measured at three different concentrations of 2-AG. Data show means ± S.E. ($n = 9–30$) from 3–10 independent experiments. **, $p < 0.01$; ***, $p < 0.001$, one-way analysis of variance followed by Dunnett's post hoc test.

TABLE 8

Potency (pEC_{50}) and efficacy (E_{max}) values for different concentrations of the allosteric modulator Pepcan-12 and the inverse agonist SR141716 in combination with the agonists HU-210, WIN55,212, and 2-AG in cAMP accumulation and [^{35}S]GTPγS binding assays

Values were estimated by nonlinear regression and represent the mean ± S.E. pEC_{50} and E_{max} values from curves of different concentrations of SR141716 in combination with WIN55,212-2 in the cAMP accumulation assay are listed in the legend of Fig. 10. *, $p < 0.05$; **, $p < 0.01$; ***, $p < 0.001$, one-way analysis of variance followed by Dunnett's post hoc test; #, $p < 0.05$, Student's unpaired t test.

Assay (agonist) + parameter	[Competitor], 0 nM	[Competitor], 1 nM	[Competitor], 100 nM	[Competitor], 1 μM
cAMP (WIN55,212-2)				
pEC_{50}	7.07 ± 0.05[a]	6.99 ± 0.06[a]	6.98 ± 0.12[a]	7.02 ± 0.08[a]
E_{max}	468.2 ± 16.3[a]	370.1 ± 14.6[a***]	301.3 ± 22.1[a***]	255.1 ± 11[a***]
cAMP (2-AG)				
pEC_{50}	7.08 ± 0.15[a]	7.33 ± 0.15[a]	7.30 ± 0.38[a]	7.78 ± 0.06[a]
E_{max}	620.8 ± 39.8[a]	420.9 ± 23.7[a***]	435 ± 59.7[a**]	328 ± 5.8[a***]
pEC_{50}	7.15 ± 0.15[b]		6.23 ± 0.27[b#]	-
E_{max}	622.2 ± 40.5[b]		636.5 ± 78.2[b]	-
[^{35}S]GTPγS (HU-210)				
pEC_{50}	7.79 ± 0.25[a]	7.79 ± 0.17[a]	7.91 ± 0.26[a]	-
E_{max}	265.6 ± 16.6[a]	214.0 ± 7.2[a***]	221.5 ± 8.2[a*]	-
pEC_{50}	8.61 ± 0.9[b]	7.5 ± 0.23[b]	6.21 ± 0.15[b*]	-
E_{max}	187.6 ± 8.5[b]	186.2 ± 9.5[b]	186.9[b,c]	-

[a] Pepcan-12.
[b] SR141716.
[c] Constrained E_{max} value for nonlinear fitting procedure.

immunoaffinity MS assay procedure. Furthermore, we were not able to detect the N-terminally truncated peptide VDPVNFKLLSH reported to occur in the mouse brain (10, 12). The identification of the Pepcan family in hamster brain extracts confirmed our results obtained with mouse brain tissue. That we did not detect any Pepcans in rat brain tissue using this immunoaffinity MS method was most likely due to the decreased binding affinity of our mAbs toward the rat Pepcans, as indicated by a 14-fold decreased binding affinity of the mAb 1A12 for the rat sequence after ACN extraction (Table 7).

Because of the immunoaffinity enrichment step, we were able to identify, for the first time, Pepcan-14 to -23 in brain extracts and plasma samples. It seems as if Pepcan-12, -14, -15, -17, and -20 are the most relevant endogenous Pepcans occurring in mouse brain and mouse/human plasma samples. In comparison with conventional LC-MS/MS methods, the immunoaffinity step provides a significant enrichment of Pepcans and increased signal/noise ratios, resulting in increased sensitivity and in the reduction of ion suppression mediated by highly abundant proteins and peptides (60–64).

Cannabinoid Receptor Binding Interactions of Pepcans—The Pepcans identified *ex vivo* were investigated for their CB_1 binding properties. We used both a classical radioligand assay and a newly developed assay with the Pepcan-12 derivative Pepcan-F4, containing a C-terminally attached fluorescein via spacer molecules. At 1 μM, Pepcan-12, -14, and -20 were found to moderately displace [^{3}H]CP55,940 and [^{3}H]WIN55,212-2 from CB_1 receptors. Pepcan-12 showed the strongest displacement of both radioligands characterized by a saturable but only partial receptor binding, thus suggesting an interaction with an allosteric binding site. Binding data were fitted with the allosteric TCM model, revealing similar pK_B values of Pepcan-12 for both radioligands at the putative allosteric binding site. The cooperativity factor α, which describes the magnitude of the allosteric change in ligand affinity that occurs between two conformationally linked sites when both ligands are bound (39), was in both cases less than 1, indicating a negative allosteric modulation. Although these results could theoretically also be in agreement with our aggregation theory, at higher Pepcan concentrations, the dissociation kinetic data clearly favor an allosteric binding site for Pepcan-12. Indeed, only ligands that bind to a topographically distinct site at the receptor can enhance (or reduce) the dissociation of an orthosteric ligand in the isotopic dilution approach used (39). The biphasic dissociation kinetics of [^{3}H]CP55,940 also indicates the presence of at least two receptor conformations (65) and was already discussed in detail by Price *et al.* (16). Pepcan-12 increased the dissociation rate constants for both the fast and slow components of [^{3}H]CP55,940 binding. This is in line with a conformational change induced by Pepcan-12 binding to an allosteric site that decreases the agonist (CP55,940) affinity for the orthosteric binding site at the CB_1 receptor.

Experiments with the fluorescently labeled Pepcan-F1 to -F4, which were derived from Pepcan-12, show that N-terminal derivatization of Pepcan-12 abolished CB receptor binding. In contrast, C-terminal derivatization had comparatively little effect, as long as the fluorophore was not attached to the peptide directly but rather via a spacer molecule. These results suggest that the N terminus of the peptide is of particular importance for CB receptor binding interactions. Thus, the differential interactions of Pepcan-12 to -20 may be determined by particular amino acid residues. Nonetheless, the less strong and only partial displacement by the two C-terminally truncated versions of Pepcan-12, RVDPVNF and RVDPVNFKLL, indicates that the whole peptide sequence, including the C terminus, is probably involved to different extents in CB_1 receptor binding interactions. Whereas Pepcan-12, -14, -15, and -17 interacted strongly with the Pepcan-F4 binding site in CB_1 receptors, the longest Pepcan tested (Pepcan-20) did not displace Pepcan-F4. Although the nonspecific Pepcan-F4 binding was subtracted in all of the Pepcan inhibition curves, a residual 15–25% of fluorescence remained. Possible explanations for this may either be *in vitro* peptide aggregation at higher concentrations or that the fluorescent label, including spacer molecules, modifies the Pepcan-12 binding behavior by increasing its binding affinity for CB_1 receptors. Alternatively, potential peptide aggregation at the CB_1 receptor may play a role. Because of conformational linkage between the two binding

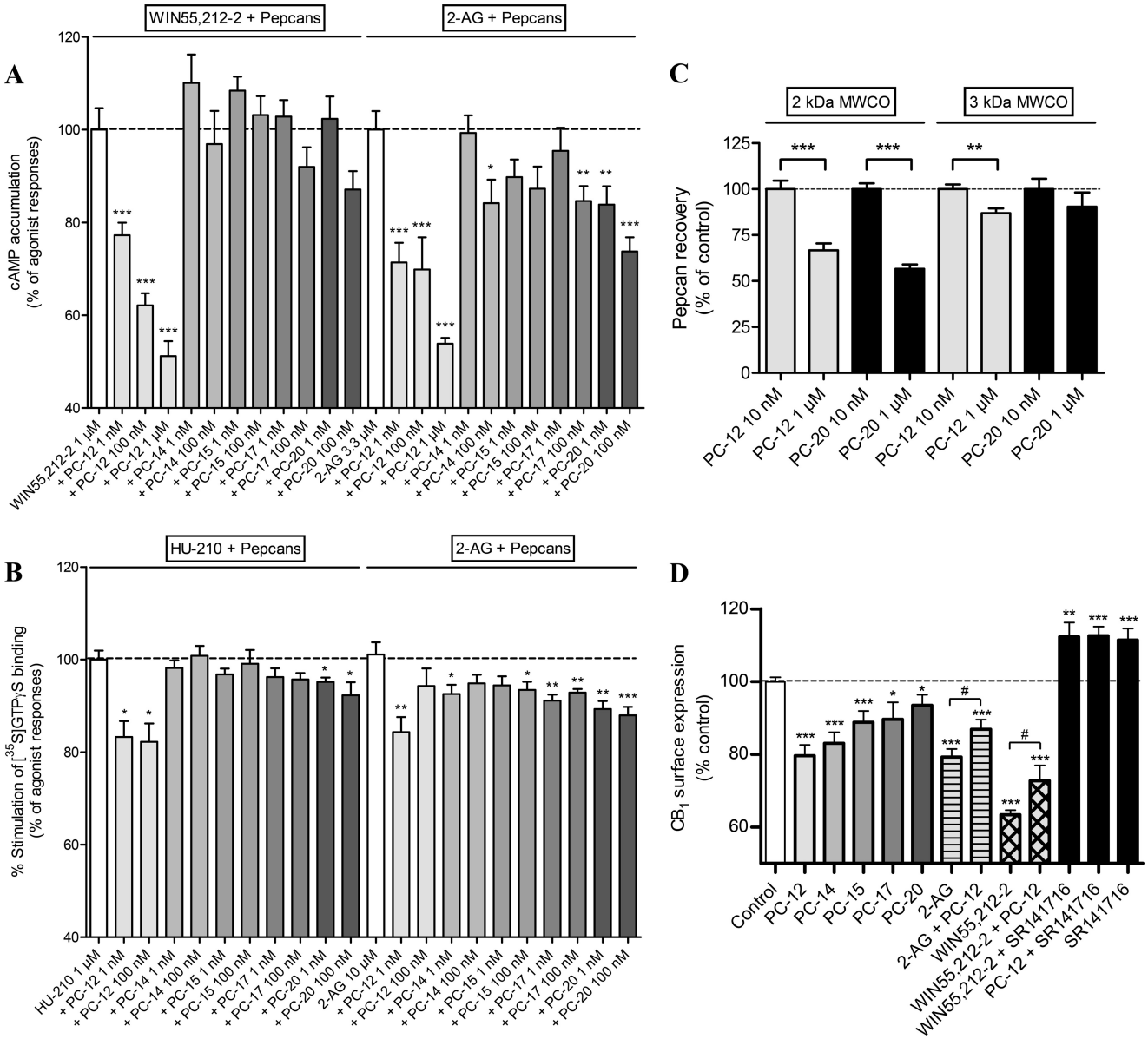

FIGURE 11. *A* and *B*, influence of Pepcan-12 to -20 on cAMP accumulation and [^{35}S]GTPγS binding induced by WIN55,212-2, 2-AG, and HU-210. Data show means ± S.E. ($n = 9–12$) from 3–4 independent experiments (*, $p < 0.05$; **, $p < 0.01$; ***, $p < 0.001$, Student's unpaired *t* test of Pepcan-treated *versus* vehicle control-treated cannabinoid receptor agonist groups). *C*, aggregation measured for Pepcan-12 and Pepcan-20. Results show the peptide recovery of a low (10 nM) and a high (1 μM) concentration of Pepcan-12 and -20 in RPMI1640 medium after incubation and subsequent centrifugation by ultrafiltration and quantification by competitive ELISA. Results were normalized to the 10 nM recovery of the corresponding Pepcan. Two molecular mass cut-off membranes (2000 and 3000) were used to investigate the eventual formation of lower molecular weight aggregates, such as dimers or trimers. Data show means ± S.E. ($n = 9$) from three independent experiments (*, $p < 0.05$; **, $p < 0.01$; ***, $p < 0.001$, Student's unpaired *t* test between the indicated groups). *D*, Pepcans, 2-AG, and WIN55,212-2 induce partial internalization of CB_1 receptors in CHO-*h*CB_1 cells. In combination with 2-AG and WIN55,212-2, the induced internalization was partially reversed by Pepcan-12. All compounds were used at 1 μM. Data show means ± S.E. (*error bars*) ($n = 9$) from three independent experiments (*, $p < 0.05$; **, $p < 0.01$; ***, $p < 0.001$, Student's unpaired *t* test of compounds *versus* vehicle control; #, $p < 0.05$, *t* test between the indicated groups).

sites, the interaction between the orthosteric endocannabinoid binding site and the allosteric Pepcan binding site should be reciprocal (39). Therefore, we would expect to observe a similar partial displacement of Pepcan-F4, at least for WIN55,212-2 and CP55,940, both used in radioligand displacement experiments. However, we did not observe an increased binding of Pepcan-F4 to its binding site when co-incubated with cannabinoids. On the contrary, SR141716 induced an increase of Pepcan-F4 binding. This could be explained by probe dependence. The synthetic Organon compounds have been reported to show positive allosteric modulation of CP55,940 and negative allosteric modulation of SR141716 (16). The strong increase in Pepcan-F4 fluorescence intensity mediated by WIN55,212-2 might be due to a prominent allosteric effect, but it could also be caused by proximity interactions between the fluorophore in Pepcan-F4 and the conjugated electron system present in WIN55,212-2. Considering this together with the results obtained for CP55,940, which showed no effect on Pepcan-F4 binding, and for the endocannabinoids AEA and 2-AG, which showed only a weak increase of Pepcan-F4 binding at 10 μM, we conclude that the fluorescence labeling of Pepcan-12 might modify its binding affinity to CB_1 receptor, or there is residual

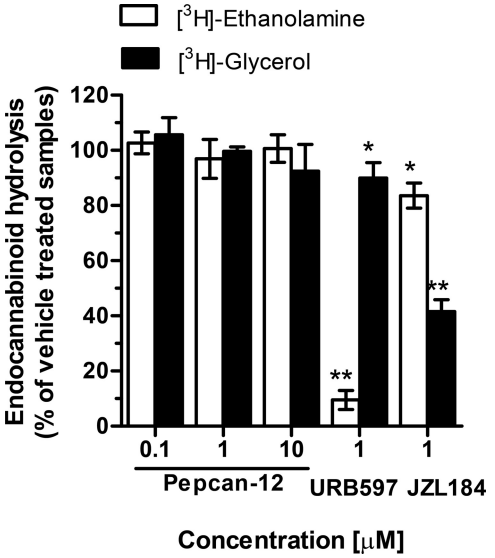

FIGURE 12. **Effect of Pepcan-12 on AEA and 2-AG hydrolysis in pig brain homogenate.** The hydrolytic products [^{3}H]ethanolamine from AEA breakdown and [^{3}H]glycerol from 2-AG breakdown were quantified. The positive controls URB597 (fatty acid amide hydrolase inhibitor) and JZL184 (monoacylglycerol lipase inhibitor) showed significant inhibition of AEA and 2-AG breakdown, respectively. Data show means ± S.D. (*error bars*) ($n = 3$) (*, $p < 0.05$; **, $p < 0.01$, Student's unpaired *t* test of compounds *versus* vehicle control).

peptide cellular uptake via CB_1 receptors. However, a radioactively labeled Pepcan-12 molecule would be necessary to clearly investigate the reciprocal interactions between the orthosteric and allosteric binding site at the CB_1 receptor. At present, several factors, such as the sample preparation (whole cells *versus* cell membranes), molecular structure (Pepcan-12 *versus* Pepcan-F4), assay read-out (fluorescence intensity *versus* radioactive signal), and assay conditions avoid the direct comparison between the effects exerted by Pepcans on the orthosteric ligands and *vice versa*. Nonetheless, the fluorescently labeled Pepcan-F4 crucially contributed to the characterization of the CB_1 receptor interaction of Pepcans and represents a versatile tool to further explore Pepcan binding to CB receptors in different biological matrixes. In addition, we also show that Pepcan-F4 apparently selectively and rapidly (within 5 min) binds to both CB_1 and CB_2 receptors, as indicated by the lack of binding in non-transfected cells or cells transfected with other cannabinoid-related receptors. That Pepcan-F4 binds to CB_2 receptors is intriguing and in conflict with a previous report on the apparent CB_1 receptor selectivity of Pepcan-12 (10). We will address the Pepcan CB_2 receptor interactions and possible functional effects in an independent study. Importantly, the bulk of Pepcan-F4 did not penetrate into CHO-*h*CB_1 cells, even after several h of incubation. Although in the FACS assay the nonspecific binding was higher, due to higher sensitivity, a very clear difference between CB receptor-expressing cells and cells lacking CB receptor surface expression was still visible. For class A G protein-coupled receptors, it has been shown that for peptide receptors, such as the opioid receptors, the endogenous ligands, including enkephalins (5 amino acid residues), endorphins (≥16 amino acid residues), and dynorphins (oligopeptides), appear to primarily bind to orthosteric domains in the extracellular loops of the receptors (39, 66). Therefore, the allosteric binding of Pepcans may not be in the loops of the transmembrane region but rather at the surface or extracellular region of CB_1 receptors. In the fluorescence images with Pepcan-F4, discrete regions of more strongly stained spots are visible, which may suggest peptide aggregation at specific sites. Because this staining clearly correlated with CB receptor expression and was not seen in non-transfected CHO cells, Pepcan aggregation directly occurring at CB_1 receptors or staining of oligomeric subpopulations of CB_1 receptors cannot be excluded at this point and needs further investigation. This also raises interesting questions regarding the potential differential functions of these ligands (see below). Taken together, our data suggest that Pepcans bind to an allosteric CB_1 receptor binding site topographically distinct from the orthosteric endocannabinoid site.

Quantification of Pepcans by Competitive ELISA—Because our Pepcan-specific mAbs bind to multiple members of the Pepcan family, only concentrations for these Pepcans together could be determined. The measured average Pepcan plasma levels of 6 nM were in the range of the obtained K_i values. For quantification of Pepcans from brain tissues (92 pmol/g of brain tissue) we were concerned about potential postmortem cleavage of Hb or Pepcan fragments. Already after a few min post mortem, several proteins and peptides were reported to be enzymatically degraded, resulting in a different composition of the peptidome and proteome compared with the real situation *in vivo* (67). Gomes *et al.* (10) and Gelman *et al.* (12) used microwave-irradiated mice to prevent postmortem protein and neuropeptide degradation and suggested a possible role of global ischemia in the up-regulation of VDPVNFKLLSH and Pepcan-12 (10, 12, 68, 69). Additionally, they reported VDPVNFKLLSH to be much more abundant in brain extracts that were not subjected to microwave irradiation (10, 68). Sköld *et al.* (67) reported several drawbacks of microwave irradiation and introduced a novel method using rapid and conductive heat transfer on brain tissue prior to the extraction procedure. For our quantification experiments, brain tissues from conventionally sacrificed mice were frozen in liquid nitrogen within 3 min post mortem.

Although Pepcan-12, -14, -15, -17, and -20 were also detected in plasma, we cannot exclude the possibility that Pepcans that showed weak signal/noise ratios in immunoaffinity MS spectra, such as Pepcan-16, -18, and -19, may be post-mortem cleavage artifacts of longer Pepcan precursor molecules. However, indirect confirmation for the existence of N-terminal extended Pepcans is also provided by the fact that Hb α chain fragments, such as AGHLDDLPGALSA, AGHLDDLPGALSAL, ANAAGHLDDLPGALSA, ANAAGHLDDLPGALSAL, ADALANAAGHLDDLPGALSA, and ADALANAAGHLDDLPGALSAL, have been reported to occur in mouse brain and blood (10, 12), indicating the presence of N-terminal cleavage sites for Pepcan-20 and -21 (Table 3). Additionally, LSDLHAHKL was detected, supporting our hypothesis that longer Pepcans (in this case Pepcan-21) could be processed to Pepcan-12. Because our mAbs are not specific for any single Pepcan, the developed competitive ELISA is not suitable for individual quantifications. Therefore, we have considered developing a quantitative immunoaffinity MS/MS approach for the quanti-

fication of single Pepcans using synthetic stable isotope-labeled peptide standards together with multiple reaction monitoring (25, 60, 61).

It is tempting to speculate that the different N-terminally truncated Pepcan species found endogenously in rodent brain tissues as well as mouse and human plasma represent precursor molecules of Pepcan-12, which is apparently the most abundant and functionally most efficacious member. However, different Pepcans may exert additional yet unknown effects at CB_1 receptors and possibly also CB_2 receptors (studies on CB_2 receptors are ongoing in our laboratory). Whereas Pepcan-12 appears to be abundant in brain tissue, based on our immunoaffinity MS experiments, and is detectable by conventional less sensitive LC-MS/MS approaches (10, 12), comparable amounts of all major Pepcans were found to occur in plasma. Using our mAbs, we will be able to address the issue of whether Pepcans are synthesized within the brain or are transported there from the periphery. Gelman *et al.* (12) have suggested that the Hb-derived peptides described by them are specifically produced in the brain. Because we did not use perfused mouse brains, we cannot draw conclusions from the presented data but favor the hypothesis that Pepcans in the brain are produced there. The fact that we identified a broader range of Pepcan species in brain extracts than in plasma could be due to the overall higher concentration of Pepcans in the brain extracts or differential processing.

Pepcans Act as Negative Allosteric Modulators at CB_1 Receptors—It is known that the way in which an allosteric ligand modulates the affinity of an orthosteric ligand does not necessary coincide with its effects on orthosteric ligand efficacy (39). In agreement with the CB_1 receptor binding data, Pepcan-12 acted as a negative allosteric modulator of cannabinoid and endocannabinoid efficacy in assays investigating CB_1 receptor-induced G protein signaling activation. We obtained conclusive data in both cAMP accumulation and [^{35}S]GTPγS binding assays using CHO-*h*CB_1 cells and mouse cerebellar extracts. Although the inverse agonist SR141716 competitively inhibited the potency of different cannabinoid agonists, Pepcan-12 reduced the efficacy without altering potency, thus clearly indicating a negative allosteric interaction. Why only a maximal effect of 20–50% could be achieved remains to be elucidated. A possible explanation may be a "ceiling effect," which has been reported for allosteric modulators, where the saturation of the allosteric site is determined by the cooperativity between the orthosteric and allosteric ligands (57). Therefore, beyond a specific threshold concentration, allosteric modulators cannot produce any further modulatory effects of the orthosteric ligands (66). Furthermore, the possibility cannot be excluded that Pepcan-12 only targets a subpopulation of CB receptors (*e.g.* homodimers or oligomers).

Interestingly, although Pepcan-20 was not able to displace the fluorescent derivative Pepcan-F4 from CB_1 receptors, it induced a significant displacement of [^{3}H]CP55,940 and [^{3}H]WIN55,212-2, thus showing that Pepcan-F4 binds differently to CB_1 receptors than native Pepcans. Additionally, Pepcan-20 decreased the agonist-induced cAMP accumulation and [^{35}S]GTPγS binding like Pepcan-12, although less strongly. Why Pepcan-20 was not able to displace Pepcan-F4 from CB_1 receptors is not yet clear. A possible explanation could be that Pepcan-20 binds to a distinct or partially overlapping binding site from Pepcan-F4. This may suggest that the peptide elongation by three additional amino acids from Pepcan-17 (which displace Pepcan-F4 very efficiently) has a great impact on the binding affinity and/or site. This needs to be investigated using a radiolabeled Pepcan-12 molecule. Nonetheless, Pepcan-20 may play a physiological role because its functional effect is qualitatively identical to that of Pepcan-12.

In both assays investigating G protein signaling, Pepcans did not elicit any response by themselves but only modulated the effects induced by orthosteric ligands. Because Pepcan-12 was reported to act as an agonist (10) and hemopressin as an inverse agonist (8, 9) at CB_1 receptors, we also investigated a potentially G protein-independent pathway. We decided to investigate the agonist-induced receptor internalization of CB_1 receptors in a transfected cell line because this mechanism may be independent of G proteins (31, 70). Although Pepcan-12, -14, -15, -17, and -20 apparently behaved as partial agonists in the CB_1 receptor internalization assay using CHO-*h*CB_1 cells, they reversed the 2-AG- and WIN55,212-2-induced internalization by 25–35%. Whether this Pepcan-induced receptor internalization is merely an artificial *in vitro* effect or has some relevance *in vivo* remains to be elucidated. If Pepcans behave as partial agonists in other CB_1 receptor signaling pathways (*e.g.* via arrestins) needs to be investigated in further studies. Pepcan-12 has been shown to mediate a sustained increase in Ca^{2+} levels and neurite outgrowth in Neuro2A cells and to increase ERK phosphorylation in HEK293 cells expressing *myc*-tagged CB_1 receptors (10). In our laboratory, we were unable to detect significant Ca^{2+} transients with Pepcans in CHO-*h*CB_1 and Neuro2A cells using fluorescent imaging plate reader calcium assays (data not shown). On the other hand, $G_{i/o}$ and G_s pathways are well established and predominant in CB_1 receptors (73). In our hands, Pepcans clearly behaved as negative allosteric modulators on the orthosteric binding site for these pathways in two different experimental setups. From our data, we can conclude that the actions of Pepcans are exerted via a novel allosteric binding site at CB_1 receptors.

Conclusions—The discovery of a family of endogenous peptides generated from α-hemoglobin that act as negative allosteric modulators at CB_1 receptors provides new evidence for additional players in the endocannabinoid system. Importantly, the negative allosteric effects mediated by Pepcans occur at nanomolar concentrations, which are in agreement with the concentrations detected in mouse brain and human plasma samples. As previously emphasized (71), allosteric modulation heralds a new approach to the manipulation of the endocannabinoid system for therapeutic benefit; it promises to augment the existing portfolio of known CB_1 receptor ligands, such as direct agonists and competitive antagonists. Because Pepcans are the first endogenous allosteric modulators described, it will be interesting to see whether the small synthetic allosteric modulators reported previously (15–18) target the same binding sites as Pepcans at CB_1 receptors. Finally, the anti-Pepcan mAbs and ELISA described in this study represent first important tools for studying the role of Pepcans in cellular and phys-

iological systems as well as for their quantification in disease models.

Acknowledgment—We thank Alexandra Schubert for performing some radioligand displacement experiments.

REFERENCES

1. Matsuda, L. A., Lolait, S. J., Brownstein, M. J., Young, A. C., and Bonner, T. I. (1990) Structure of a cannabinoid receptor and functional expression of the cloned cDNA. *Nature* **346,** 561–564
2. Munro, S., Thomas, K. L., and Abu-Shaar, M. (1993) Molecular characterization of a peripheral receptor for cannabinoids. *Nature* **365,** 61–65
3. Pertwee, R. G., Howlett, A. C., Abood, M. E., Alexander, S. P., Di Marzo, V., Elphick, M. R., Greasley, P. J., Hansen, H. S., Kunos, G., Mackie, K., Mechoulam, R., and Ross, R. A. (2010) International Union of Basic and Clinical Pharmacology. LXXIX. Cannabinoid receptors and their ligands. Beyond CB_1 and CB_2. *Pharmacol. Rev.* **62,** 588–631
4. Mackie, K. (2006) Cannabinoid receptors as therapeutic targets. *Annu. Rev. Pharmacol. Toxicol.* **46,** 101–122
5. Hanus, L. O. (2009) Pharmacological and therapeutic secrets of plant and brain (endo)cannabinoids. *Med. Res. Rev.* **29,** 213–271
6. Di Marzo, V. (2008) Targeting the endocannabinoid system. To enhance or reduce? *Nat. Rev. Drug Discov.* **7,** 438–455
7. Pacher, P., Bátkai, S., and Kunos, G. (2006) The endocannabinoid system as an emerging target of pharmacotherapy. *Pharmacol. Rev.* **58,** 389–462
8. Heimann, A. S., Gomes, I., Dale, C. S., Pagano, R. L., Gupta, A., de Souza, L. L., Luchessi, A. D., Castro, L. M., Giorgi, R., Rioli, V., Ferro, E. S., and Devi, L. A. (2007) Hemopressin is an inverse agonist of CB1 cannabinoid receptors. *Proc. Natl. Acad. Sci. U.S.A.* **104,** 20588–20593
9. Dodd, G. T., Mancini, G., Lutz, B., and Luckman, S. M. (2010) The peptide hemopressin acts through CB1 cannabinoid receptors to reduce food intake in rats and mice. *J. Neurosci.* **30,** 7369–7376
10. Gomes, I., Grushko, J. S., Golebiewska, U., Hoogendoorn, S., Gupta, A., Heimann, A. S., Ferro, E. S., Scarlata, S., Fricker, L. D., and Devi, L. A. (2009) Novel endogenous peptide agonists of cannabinoid receptors. *FASEB J.* **23,** 3020–3029
11. Gomes, I., Dale, C. S., Casten, K., Geigner, M. A., Gozzo, F. C., Ferro, E. S., Heimann, A. S., and Devi, L. A. (2010) Hemoglobin-derived peptides as novel type of bioactive signaling molecules. *AAPS J.* **12,** 658–669
12. Gelman, J. S., Sironi, J., Castro, L. M., Ferro, E. S., and Fricker, L. D. (2010) Hemopressins and other hemoglobin-derived peptides in mouse brain. Comparison between brain, blood, and heart peptidome and regulation in Cpefat/fat mice. *J. Neurochem.* **113,** 871–880
13. Reggio, P. H. (2005) Cannabinoid receptors and their ligands. Ligand-ligand and ligand-receptor modeling approaches. *Handb. Exp. Pharmacol.* **168,** 247–281
14. Scrima, M., Di Marino, S., Grimaldi, M., Mastrogiacomo, A., Novellino, E., Bifulco, M., and D'Ursi, A. M. (2010) Binding of the hemopressin peptide to the cannabinoid CB1 receptor. Structural insights. *Biochemistry* **49,** 10449–10457
15. Horswill, J. G., Bali, U., Shaaban, S., Keily, J. F., Jeevaratnam, P., Babbs, A. J., Reynet, C., and Wong Kai In, P. (2007) PSNCBAM-1, a novel allosteric antagonist at cannabinoid CB1 receptors with hypophagic effects in rats. *Br. J. Pharmacol.* **152,** 805–814
16. Price, M. R., Baillie, G. L., Thomas, A., Stevenson, L. A., Easson, M., Goodwin, R., McLean, A., McIntosh, L., Goodwin, G., Walker, G., Westwood, P., Marrs, J., Thomson, F., Cowley, P., Christopoulos, A., Pertwee, R. G., and Ross, R. A. (2005) Allosteric modulation of the cannabinoid CB1 receptor. *Mol. Pharmacol.* **68,** 1484–1495
17. Navarro, H. A., Howard, J. L., Pollard, G. T., and Carroll, F. I. (2009) Positive allosteric modulation of the human cannabinoid (CB) receptor by RTI-371, a selective inhibitor of the dopamine transporter. *Br. J. Pharmacol.* **156,** 1178–1184
18. Piscitelli, F., Ligresti, A., La Regina, G., Coluccia, A., Morera, L., Allarà, M., Novellino, E., Di Marzo, V., and Silvestri, R. (2012) Indole-2-carboxamides as allosteric modulators of the cannabinoid CB_1 receptor. *J. Med. Chem.* **55,** 5627–5631
19. Devlin, M. G., Pfeiffer, B., Flanagan, B., Beyer, R. L., Cocks, T. M., and Fairlie, D. P. (2007) Hepta- and octapeptide agonists of protease-activated receptor 2. *J. Pept. Sci.* **13,** 856–861
20. Tamborrini, M., Werz, D. B., Frey, J., Pluschke, G., and Seeberger, P. H. (2006) Anti-carbohydrate antibodies for the detection of anthrax spores. *Angew. Chem. Int. Ed. Engl.* **45,** 6581–6582
21. Tamborrini, M., Mueller, M. S., Stoffel, S. A., Westerfeld, N., Vogel, D., Boato, F., Zurbriggen, R., Robinson, J. A., and Pluschke, G. (2009) Design and preclinical profiling of a *Plasmodium falciparum* MSP-3-derived component for a multivalent virosomal malaria vaccine. *Malar. J.* **8,** 314
22. Poetz, O., Ostendorp, R., Brocks, B., Schwenk, J. M., Stoll, D., Joos, T. O., and Templin, M. F. (2005) Protein microarrays for antibody profiling. Specificity and affinity determination on a chip. *Proteomics* **5,** 2402–2411
23. Kurzeder, C., Koppold, B., Sauer, G., Pabst, S., Kreienberg, R., and Deissler, H. (2007) CD9 promotes adeno-associated virus type 2 infection of mammary carcinoma cells with low cell surface expression of heparan sulfate proteoglycans. *Int. J. Mol. Med.* **19,** 325–333
24. Hoeppe, S., Schreiber, T. D., Planatscher, H., Zell, A., Templin, M. F., Stoll, D., Joos, T. O., and Poetz, O. (2011) Targeting peptide termini, a novel immunoaffinity approach to reduce complexity in mass spectrometric protein identification. *Mol. Cell Proteomics* **10,** M110.002857
25. Whiteaker, J. R., Zhao, L., Anderson, L., and Paulovich, A. G. (2010) An automated and multiplexed method for high throughput peptide immunoaffinity enrichment and multiple reaction monitoring mass spectrometry-based quantification of protein biomarkers. *Mol. Cell Proteomics* **9,** 184–196
26. Gertsch, J., Leonti, M., Raduner, S., Racz, I., Chen, J. Z., Xie, X. Q., Altmann, K. H., Karsak, M., and Zimmer, A. (2008) β-Caryophyllene is a dietary cannabinoid. *Proc. Natl. Acad. Sci. U.S.A.* **105,** 9099–9104
27. Leonti, M., Casu, L., Raduner, S., Cottiglia, F., Floris, C., Altmann, K. H., and Gertsch, J. (2010) Falcarinol is a covalent cannabinoid CB1 receptor antagonist and induces pro-allergic effects in skin. *Biochem. Pharmacol.* **79,** 1815–1826
28. Chicca, A., Marazzi, J., and Gertsch, J. (2012) The antinociceptive triterpene β-amyrin inhibits 2-arachidonoylglycerol (2-AG) hydrolysis without directly targeting CB receptors. *Br. J. Pharmacol.* 10.1111/j.1476–5381.2012.02059.x
29. Leach, K., Sexton, P. M., and Christopoulos, A. (2011) *Curr. Protoc. Pharmacol.*, Chapter 1, Unit 1.22
30. Massa, F., Mancini, G., Schmidt, H., Steindel, F., Mackie, K., Angioni, C., Oliet, S. H., Geisslinger, G., and Lutz, B. (2010) Alterations in the hippocampal endocannabinoid system in diet-induced obese mice. *J. Neurosci.* **30,** 6273–6281
31. Kleyer, J., Nicolussi, S., Taylor, P., Simonelli, D., Furger, E., Anderle, P., and Gertsch, J. (2012) Cannabinoid receptor trafficking in peripheral cells is dynamically regulated by a binary biochemical switch. *Biochem. Pharmacol.* **83,** 1393–1412
32. Cheng, Y., and Prusoff, W. H. (1973) Relationship between the inhibition constant (K1) and the concentration of inhibitor that causes 50 per cent inhibition (I_{50}) of an enzymatic reaction. *Biochem. Pharmacol.* **22,** 3099–3108
33. Neubig, R. R., Spedding, M., Kenakin, T., and Christopoulos, A. (2003) International Union of Pharmacology Committee on Receptor Nomenclature and Drug Classification. XXXVIII. Update on terms and symbols in quantitative pharmacology. *Pharmacol. Rev.* **55,** 597–606
34. Arunlakshana, O., and Schild, H. O. (1959) Some quantitative uses of drug antagonists. *Br. J. Pharmacol. Chemother.* **14,** 48–58
35. Christopoulos, A., and Kenakin, T. (2002) G protein-coupled receptor allosterism and complexing. *Pharmacol. Rev.* **54,** 323–374
36. Zhou, H., Wang, Y., Wang, W., Jia, J., Li, Y., Wang, Q., Wu, Y., and Tang, J. (2009) Generation of monoclonal antibodies against highly conserved antigens. *PLoS ONE* **4,** e6087
37. Fowler, C. J. (2008) "The tools of the trade." An overview of the pharmacology of the endocannabinoid system. *Curr. Pharm. Des.* **14,** 2254–2265
38. Christopoulos, A. (2002) Allosteric binding sites on cell surface receptors. Novel targets for drug discovery. *Nat. Rev. Drug Discov.* **1,** 198–210
39. May, L. T., Leach, K., Sexton, P. M., and Christopoulos, A. (2007) Allo-

steric modulation of G protein-coupled receptors. *Annu. Rev. Pharmacol. Toxicol.* **47,** 1–51
40. Lunelli, L., Zuliani, P., and Baldini, G. (1994) Evidence of hemoglobin dissociation. *Biopolymers* **34,** 747–757
41. Mrabet, N. T., Shaeffer, J. R., McDonald, M. J., and Bunn, H. F. (1986) Dissociation of dimers of human hemoglobins A and F into monomers. *J. Biol. Chem.* **261,** 1111–1115
42. DeSilva, B., Smith, W., Weiner, R., Kelley, M., Smolec, J., Lee, B., Khan, M., Tacey, R., Hill, H., and Celniker, A. (2003) Recommendations for the bioanalytical method validation of ligand-binding assays to support pharmacokinetic assessments of macromolecules. *Pharm. Res.* **20,** 1885–1900
43. Maple, L., Lathrop, R., Bozich, S., Harman, W., Tacey, R., Kelley, M., and Danilkovitch-Miagkova, A. (2004) Development and validation of ELISA for herceptin detection in human serum. *J. Immunol. Methods* **295,** 169–182
44. Watson, C., Jenkinson, S., Kazmierski, W., and Kenakin, T. (2005) The CCR5 receptor-based mechanism of action of 873140, a potent allosteric noncompetitive HIV entry inhibitor. *Mol. Pharmacol.* **67,** 1268–1282
45. Zahn, K., Eckstein, N., Tränkle, C., Sadée, W., and Mohr, K. (2002) Allosteric modulation of muscarinic receptor signaling. Alcuronium-induced conversion of pilocarpine from an agonist into an antagonist. *J. Pharmacol. Exp. Ther.* **301,** 720–728
46. Urwyler, S., Mosbacher, J., Lingenhoehl, K., Heid, J., Hofstetter, K., Froestl, W., Bettler, B., and Kaupmann, K. (2001) Positive allosteric modulation of native and recombinant γ-aminobutyric acid(B) receptors by 2,6-di-*tert*-butyl-4-(3-hydroxy-2,2-dimethyl-propyl)-phenol (CGP7930) and its aldehyde analog CGP13501. *Mol. Pharmacol.* **60,** 963–971
47. Litschig, S., Gasparini, F., Rueegg, D., Stoehr, N., Flor, P. J., Vranesic, I., Prézeau, L., Pin, J. P., Thomsen, C., and Kuhn, R. (1999) CPCCOEt, a noncompetitive metabotropic glutamate receptor 1 antagonist, inhibits receptor signaling without affecting glutamate binding. *Mol. Pharmacol.* **55,** 453–461
48. Howlett, A. C., and Fleming, R. M. (1984) Cannabinoid inhibition of adenylate cyclase. Pharmacology of the response in neuroblastoma cell membranes. *Mol. Pharmacol.* **26,** 532–538
49. Howlett, A. C., Johnson, M. R., Melvin, L. S., and Milne, G. M. (1988) Nonclassical cannabinoid analgetics inhibit adenylate cyclase. Development of a cannabinoid receptor model. *Mol. Pharmacol.* **33,** 297–302
50. Felder, C. C., Veluz, J. S., Williams, H. L., Briley, E. M., and Matsuda, L. A. (1992) Cannabinoid agonists stimulate both receptor- and non-receptor-mediated signal transduction pathways in cells transfected with and expressing cannabinoid receptor clones. *Mol. Pharmacol.* **42,** 838–845
51. Howlett, A. C., Qualy, J. M., and Khachatrian, L. L. (1986) Involvement of Gi in the inhibition of adenylate cyclase by cannabimimetic drugs. *Mol. Pharmacol.* **29,** 307–313
52. Felder, C. C., Joyce, K. E., Briley, E. M., Glass, M., Mackie, K. P., Fahey, K. J., Cullinan, G. J., Hunden, D. C., Johnson, D. W., Chaney, M. O., Koppel, G. A., and Brownstein, M. (1998) LY320135, a novel cannabinoid CB1 receptor antagonist, unmasks coupling of the CB1 receptor to stimulation of cAMP accumulation. *J. Pharmacol. Exp. Ther.* **284,** 291–297
53. Glass, M., and Felder, C. C. (1997) Concurrent stimulation of cannabinoid CB1 and dopamine D2 receptors augments cAMP accumulation in striatal neurons. Evidence for a G_s linkage to the CB1 receptor. *J. Neurosci.* **17,** 5327–5333
54. Maneuf, Y. P., and Brotchie, J. M. (1997) Paradoxical action of the cannabinoid WIN 55,212-2 in stimulated and basal cyclic AMP accumulation in rat globus pallidus slices. *Br J. Pharmacol.* **120,** 1397–1398
55. Bonhaus, D. W., Chang, L. K., Kwan, J., and Martin, G. R. (1998) Dual activation and inhibition of adenylyl cyclase by cannabinoid receptor agonists. Evidence for agonist-specific trafficking of intracellular responses. *J. Pharmacol. Exp. Ther.* **287,** 884–888
56. Calandra, B., Portier, M., Kernéis, A., Delpech, M., Carillon, C., Le Fur, G., Ferrara, P., and Shire, D. (1999) Dual intracellular signaling pathways mediated by the human cannabinoid CB1 receptor. *Eur. J. Pharmacol.* **374,** 445–455
57. Keov, P., Sexton, P. M., and Christopoulos, A. (2011) Allosteric modulation of G protein-coupled receptors. A pharmacological perspective. *Neuropharmacology* **60,** 24–35
58. Pertwee, R. G. (2005) Pharmacological actions of cannabinoids. *Handb. Exp. Pharmacol.* **168,** 1–51
59. Howlett, A. C., and Mukhopadhyay, S. (2000) Cellular signal transduction by anandamide and 2-arachidonoylglycerol. *Chem. Phys. Lipids* **108,** 53–70
60. Anderson, N. L., Anderson, N. G., Haines, L. R., Hardie, D. B., Olafson, R. W., and Pearson, T. W. (2004) Mass spectrometric quantitation of peptides and proteins using stable isotope standards and capture by anti-peptide antibodies (SISCAPA). *J. Proteome Res.* **3,** 235–244
61. Whiteaker, J. R., Zhao, L., Zhang, H. Y., Feng, L. C., Piening, B. D., Anderson, L., and Paulovich, A. G. (2007) Antibody-based enrichment of peptides on magnetic beads for mass spectrometry-based quantification of serum biomarkers. *Anal. Biochem.* **362,** 44–54
62. Poetz, O., Hoeppe, S., Templin, M. F., Stoll, D., and Joos, T. O. (2009) Proteome wide screening using peptide affinity capture. *Proteomics* **9,** 1518–1523
63. Nicol, G. R., Han, M., Kim, J., Birse, C. E., Brand, E., Nguyen, A., Mesri, M., FitzHugh, W., Kaminker, P., Moore, P. A., Ruben, S. M., and He, T. (2008) Use of an immunoaffinity-mass spectrometry-based approach for the quantification of protein biomarkers from serum samples of lung cancer patients. *Mol. Cell Proteomics* **7,** 1974–1982
64. Dufield, D. R., and Radabaugh, M. R. (2012) Online immunoaffinity LC/MS/MS. A general method to increase sensitivity and specificity. How do you do it and what do you need? *Methods* **56,** 236–245
65. Devlin, M. G., and Christopoulos, A. (2002) Modulation of cannabinoid agonist binding by 5-HT in the rat cerebellum. *J. Neurochem.* **80,** 1095–1102
66. Eglen, R. M., and Reisine, T. (2011) GPCRs revisited. New insights lead to novel drugs. *Pharmaceuticals* **4,** 244–272
67. Sköld, K., Svensson, M., Norrman, M., Sjögren, B., Svenningsson, P., and Andrén, P. E. (2007) The significance of biochemical and molecular sample integrity in brain proteomics and peptidomics. Stathmin 2-20 and peptides as sample quality indicators. *Proteomics* **7,** 4445–4456
68. Che, F. Y., Lim, J., Pan, H., Biswas, R., and Fricker, L. D. (2005) Quantitative neuropeptidomics of microwave-irradiated mouse brain and pituitary. *Mol. Cell Proteomics* **4,** 1391–1405
69. Bazinet, R. P., Lee, H. J., Felder, C. C., Porter, A. C., Rapoport, S. I., and Rosenberger, T. A. (2005) Rapid high energy microwave fixation is required to determine the anandamide (*N*-arachidonoylethanolamine) concentration of rat brain. *Neurochem. Res.* **30,** 597–601
70. Hsieh, C., Brown, S., Derleth, C., and Mackie, K. (1999) Internalization and recycling of the CB1 cannabinoid receptor. *J. Neurochem.* **73,** 493–501
71. Ross, R. A. (2007) Allosterism and cannabinoid CB_1 receptors. The shape of things to come. *Trends Pharmacol. Sci.* **28,** 567–572
72. Raduner, S., Majewska, A., Chen, J. Z., Xie, X. Q., Hamon, J., Faller, B., Altmann, K. H., and Gertsch, J. (2006) Alkylamides from echinacea are a new class of cannabinomimetics. Cannabinoid type 2 receptor-dependent and -independent immunomodulatory effects. *J. Biol. Chem.* **281,** 14192–14206
73. Abadji, V., Lucas-Lenard, J. M., Chin, C., and Kendall, D. A. (1999) Involvement of the carboxyl terminus of the third intracellular loop of the cannabinoid CB1 receptor in constitutive activation of G_s. *J. Neurochem.* **72,** 2032–2038